Fuel 288 (2021) 119513

Contents lists available at ScienceDirect

Fuel

journal homepage: www.elsevier.com/locate/fuel

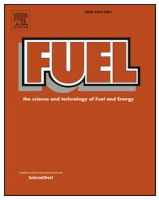

Full Length Article

Natural gamma-ray spectroscopy (NGS) as a proxy for the distribution of clay minerals and bitumen in the Cretaceous McMurray Formation, Alberta, Canada

Ruarri J. Day-Stirrat [a,*], Stephen Hillier [b,c], Anton Nikitin [a], Ronny Hofmann [a], Robert Mahood [d,1], Gilles Mertens [e]

[a] Shell International Exploration and Production Inc., Shell Technology Center Houston, 3333 Highway 6 South, Houston, TX 77082, USA
[b] The James Hutton Institute, Craigiebuckler, Aberdeen AB15 8QH, UK
[c] Department of Soil and Environment, Swedish University of Agricultural Sciences (SLU), SE-75007 Uppsala, Sweden
[d] Shell Canada, Shell Technology Center Calgary, 3655 36st. N.W., Calgary, Alberta T2L 1Y8, Canada
[e] Qmineral bvba, Gaston Geenslaan 1, B-3001 Heverlee, Belgium

ARTICLE INFO

Keywords:
Oil sands
McMurray formation
Kaolinite
Vermiculite
Kaolinite-expandable mixed-layer mineral
Natural gamma-ray spectroscopy

ABSTRACT

Detailed examination of the mineralogy of the Cretaceous McMurray Formation within a facies framework is used to assess the use of natural gamma-ray spectroscopy (NGS) and a pulsed neutron generator (PNG) tool in delineating variation in clay mineral and bitumen contents. Characterization of the mixed-layer (interstratified) clay phases in the McMurray Formation provides an improved understanding of clay interaction in bitumen processing and tailings settling behavior, important for mine planning and tailings remediation schemes. Mineral diversity in the McMurray Formation was determined on facies attributed samples using whole rock X-ray diffraction (XRD), cation exchange capacity (CEC) measurements, elemental analysis (XRF), clay size fraction (<2 μm) XRD analysis, reflected light microscopy, and cryogenic-scanning electron microscopy (cryo-SEM). Kaolinite was ubiquitous in the entire McMurray Formation with lower and middle McMurray Formation sediments also containing mixed-layered illite–smectite (I-S) with a low expandability≈ 20–30%. Upper McMurray Formation sediments by contrast had higher expandability (≈ 60–70%). In floodplain sediments of the lower McMurray Formation an additional clay mineral was quantified as a kaolinite-expandable mixed-layer (clay) mineral. The associated CEC values of this mineral are 10 times the baseline for the McMurray Formation. NGS spectra from cores showed that yields of potassium (K), uranium (U), and thorium (Th) had distinct facies associations, correlated with a clay mineral signature. The resultant indicator is capable of highlighting zones within an oil sands ore body that are empirically known, by industry, to process poorly through extraction plants. A bitumen indicator from the carbon yield derived from a PNG logging tool assesses bitumen content. NGS and PNG allow a full assessment of clay mineral (fines) and bitumen profiles, with the future prospect that these techniques could be used to assess ore and tailings behavior in near-real time.

1. Introduction

Heavy-oil and oil-sands represent an approximate 1.7 trillion-barrel reserve [17,19,1,25] of ultimately extractable hydrocarbons from the Athabasca oil sand deposit in western Canada. Open pit bitumen mining and tailings remediation operations occur at many localities north of Fort McMurray, Alberta, Canada. Prior focus has been placed on the broad geochemical aspects of the oil-sands [17] and have, via biomarker [1] and geochemical means [41], tied the biodegraded bitumen to source rocks in the eastern Canadian Rocky Mountains, with the McMurray Formation charged by oils from the Devonian/Carboniferous Exshaw Shales. The geological framework of the McMurray Formation across most of the areal extent of the bitumen mining operations in Alberta has been synthesized by Hein et al. [24] where much work has relied on field, core, and well-log analysis (e.g. [40]. These authors note the complexity across the basin where, historically, subdivisions into

* Corresponding author.
E-mail address: Ruarri.Day-Stirrat@Shell.com (R.J. Day-Stirrat).
[1] Now at: Imperial Oil, 505 Quarry Park Blvd., T2C 5N1 Calgary, Alberta, Canada.

https://doi.org/10.1016/j.fuel.2020.119513
Received 8 July 2020; Received in revised form 12 October 2020; Accepted 13 October 2020
Available online 17 December 2020

lower fluvial, middle estuarine, and upper coastal-plain successions were used and largely remain in use today (Fig. 1).

Ore processing studies have noted many associations between clay and bitumen [35,46,45] and the effects of swelling [20] and non-swelling [48] clays on bitumen extraction has been assessed. However, it seems probable that some of these studies have oversimplified the clay mineralogy of the McMurray Formation by using reference clay minerals as analogues. Conversely, some studies have recognized the complexity of some McMurray Formation clay minerals. Indeed, from a bitumen extraction and tailings management perspective efforts have been made to understand the interstratified nature of mixed-layer clays found in parts of the McMurray formation using synchrotron XRD [46] as well as more accessible laboratory based X-ray techniques [45]. These authors discussed the effect of particle size on what they quantified as various types of mixed-layer kaolinite-smectite and illite-smectite which become more evident in smaller size fractions. High resolution transmission electron microscopy employing lattice fringe imaging confirm this phase and size relationship [30]. Recently, various other techniques have been applied to characterizing the mineralogy. Surface techniques such as, Fourier Transform Infrared Spectroscopy (FTIR), have been tried and continue to be employed (e.g. [47]). Likewise inferring, surface properties (e.g. methylene blue index (MBI)) from hyperspectral data, or short-wave infrared (SWIR) or long-wave infrared (LWIR) are continuing areas of research (e.g. [16]). Nevertheless, without clear and unambiguous clay mineralogical underpinnings these methods may not yield the insights sought as continental sedimentary sequences with coals and paleosols are amongst some of the most complex of sedimentary deposits (e.g. [2] and references therein). In these soil-like settings, analysis of multiple size fractions and X-ray diffraction profile fitting are required [32,31] to fully characterize the clay mineral assemblages. Such zones in the McMurray Formation have been frequently recognized in a stratigraphic sense (Broughton, 2012) but their characterization has been limited to discussions of kaolinite presence, where in fact complex clay mineral mixed-layering is often likely.

This paper interrogates the whole rock and clay mineralogy complexity within the McMurray Formation and then attempts to link these insights to the detailed lithofacies, bitumen content, and build proxy techniques that could be used for rear-real time monitoring for example, natural gamma-ray spectroscopy (NGS) could be developed as a clay indicator. Further, neutron induced gamma-ray techniques (Pulsed Neutron Generation, PNG) could be developed as a method to assess bitumen content. However, without a detailed understanding of the associations between lithofacies and their key mineral and elemental underpinnings a framework for in-line instrumentation or near real-time monitoring of process streams or tailings lines is not a viable prospect.

1.1. Geology

Open pit bitumen mining operations occur in the McMurray Formation at the Muskeg River Mine and Jackpine Mine leases located north of Fort McMurray, Alberta, Canada and samples from these mines form the basis for this study. The eroded Devonian carbonate plane onto which the Cretaceous McMurray Formation was deposited had significant relief at deposition resulting in a McMurray Formation of variable thickness across the Athabasca region. In the heart of the paleo depositional valley [6,7] the McMurray Formation is around 100 m thick. The stratigraphic nomenclature for the Athabasca Wabiskaw-McMurray tends to be largely informal where Carrigy [8] subdivided the McMurray Formation into the lower, mostly fluvial; middle, mainly estuarine; and an upper dominantly coastal plain succession. These caveat words

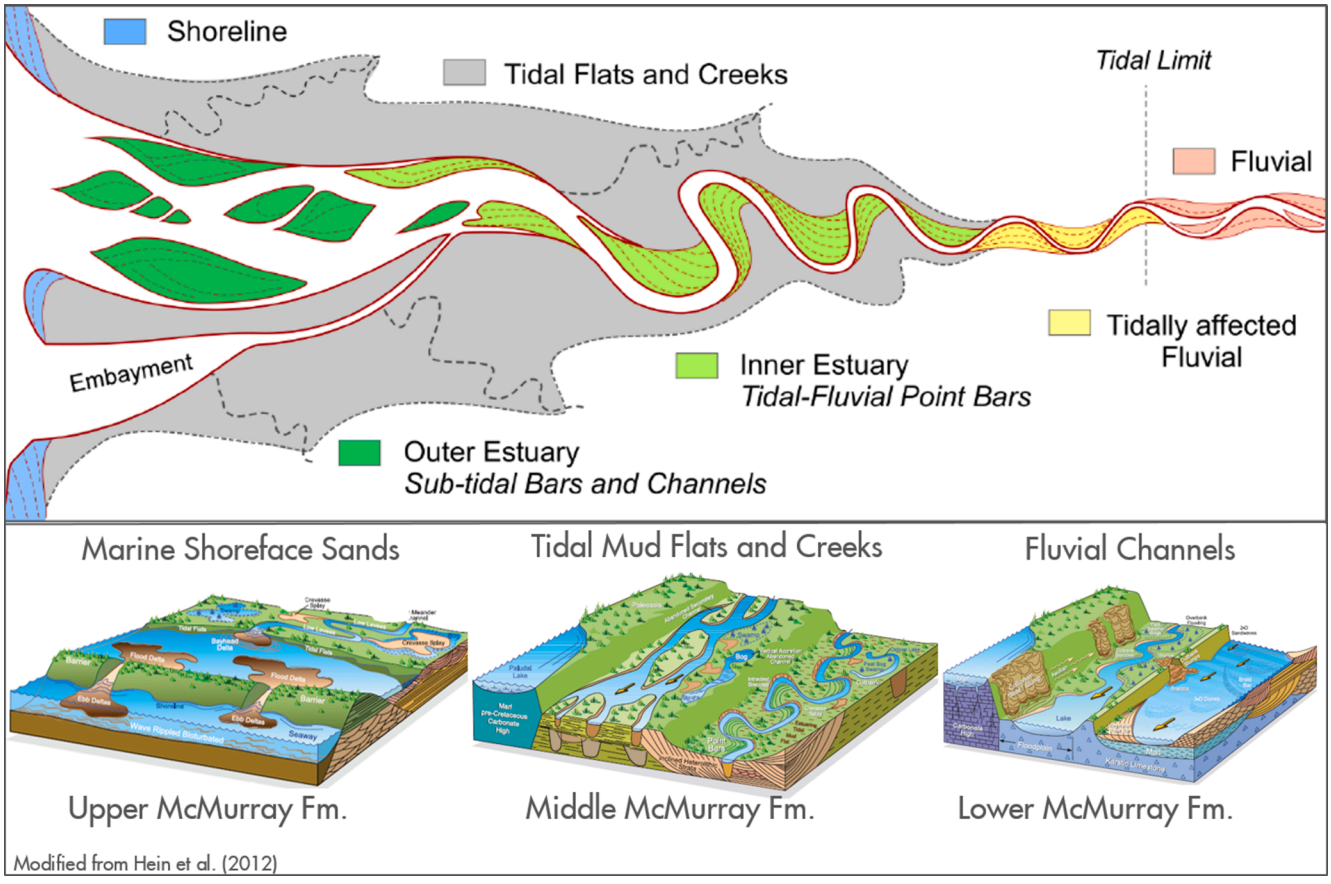

Fig. 1. Fluvial, estuarine, and marine elements comprise the Cretaceous McMurray Formation. Block diagrams modified after Hein et al. [25] show the relative size of sand packages within the three main depositional elements.

"mostly" and "mainly" emphasize the difficulties around lateral correlation, further complicated by fragmentation of the stratigraphy [24,23] resulting from multiple unconformities and truncations. Indeed, as these authors point out, the lithofacies preserved do not appear to be from a single system tract suggesting one model of deposition is insufficient. The detailed work by Nardin et al. [42] on point bars from Syncrude's Mildred Lake Mine reveal many lithotypes formed during meander loop formation. This heterogeneity leads to varying bitumen concentrations and types [17,19,18]. As a direct result of the complexity of the depositional system and the varying contributions of fluvial, estuarine, and marine depositional environments, across any one mine lease, local facies and subfacies descriptions are often used. For the Muskeg River Mine and Jackpine Mine leases, from overlying Quaternary units, through the McMurray Formation, and into the underlying Devonian approximately 90 subfacies are used [3,4]. Cores are acquired on a 100 m by 100 m spacing during a winter coring campaign and consistency in using the subfacies nomenclature is a key requirement of the mining operation.

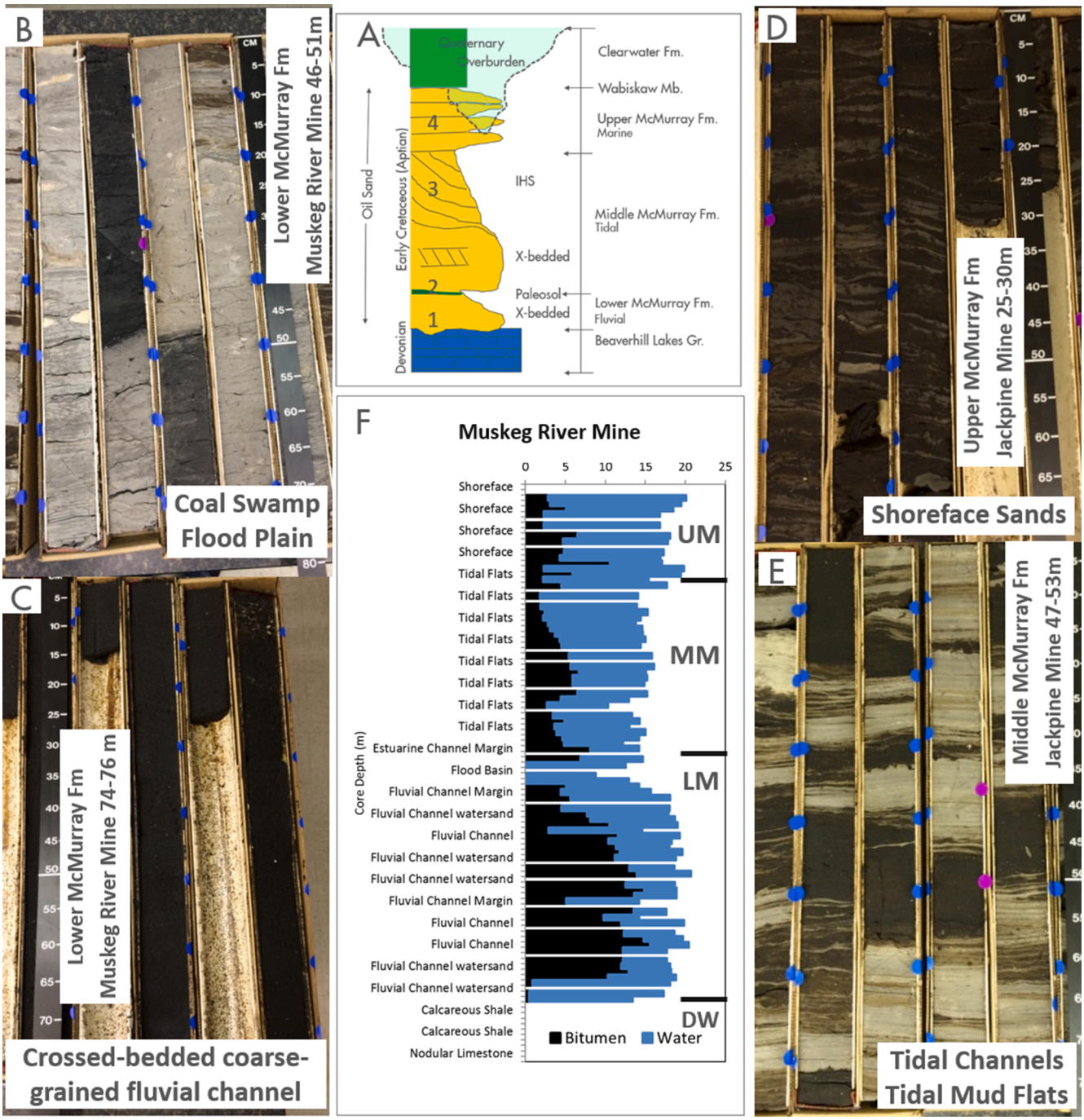

Fig. 2. Channel sands of the lower McMurray Formation are separated from the middle McMurray Formation by localized palesols, coal swamps and flood plain deposits. The upper McMurray Formation comprises shoreface sands that are easily distinguished from the inclined heterolithic structures (IHS) of the middle McMurray Formation. Cores from the Muskeg River Mine (MRM13 Cr0101) and the Jackpine Mine (JPM13 Cr 3017) are used to illustrate the facies variability. Routine analysis of the water and bitumen content (MRM13 Cr0101 core, sampling approximately 40 cm of core length) shows a typically higher bitumen content in the lower McMurray Formation (LM) than in the middle or upper McMurray Formations (MM and UM). Devonian (DW) carbonates sit unconformably below the McMurray Formation and are not considered further.

Channel sands of the lower McMurray Formation (LM) are separated from the middle McMurray Formation (MM) by localized fine-grained and low bitumen content palesols, coal swamps and flood plain deposits [11]. The upper McMurray Formation (UM) comprises horizontal shoreface sands that are easily distinguished from the inclined heterolithic structures (IHS) of the middle McMurray Formation [40,37]. Cores from the Muskeg River Mine (MRM13 Cr0101) and the Jackpine Mine (JPM13 Cr3017) are used to illustrate the facies variability (Fig. 2) along with their place in the simplified stratigraphy. Indeed, many core photographs in papers by Fustic et al. [19] and Nardin et al. [42] show features that are common across the oil sands mining leases and into this study. Routine analysis of the water and bitumen content (Muskeg River Mine core, Fig. 2) shows a typically higher bitumen content in the lower McMurray Formation (LM) than in the Middle or upper McMurray Formations (MM and UM). Few studies have examined in detail the mineralogy of the McMurray Formation in the context of depositional environments (subfacies). For the most part, past studies have lumped the subfacies of the McMurray Formation together and revealed, unsurprisingly, that quartz dominates a quartz-feldspar-rock fragment ternary system and that kaolinite does the same in a clay minerals kaolinite-illite-montmorillonite ternary system [24]. Detrital zircon U-Pb ages place the provenance of the McMurray Formation into diagenetically mature rocks of Appalachian and Greenville provinces to the east [5]. Given this provenance it seems reasonable to assume that inherited detrital clay minerals would be relatively unreactive, low swelling, illitic assemblages, and it is most likely that the more reactive clays present in the McMurray Formation are related to transformation and/or neoformation processes that are more facies specific and semi-contemporaneous with deposition.

2. Materials

A series of samples for mineralogical analyses were collected over a two-year period, 2012–2014 (Table 1, see Supplemental data). Each sample was characterized primarily in its stratigraphic occurrence and lithofacies (subfacies) context rather than mine location. Each sample was collected based on its subfacies and so contains an average of grain size or lamination contained in its subfacies description. Samples taken from core were smaller and represent more unified grain size or lamination. With the exception of samples for imaging all samples were homogenized for analysis. This yielded a mineralogy dataset that covered the entire McMurray Formation. Each sample in the various rounds of mineralogy investigation reported was assigned a subfacies description as its primary identifier placing it into the overall stratigraphy. No additions, revisions, or changes were made to the original sample descriptions provided through normal mine operations and each sample was acquired from cores or grab samples within the orebody. Two cores, one from the Muskeg River Mine (MRM13 Cr0101) assessing 37 samples and one from the Jackpine Mine (JPM13 Cr3017) assessing 30 samples were augmented with additional elemental data (X-ray fluorescence [XRF], and Instrumental Neutron Activation Analysis [INAA]) and select imaging. Further, this core was also the subject of X-ray fluorescence (XRF) core scanning. A field trial of a pulsed neutron (PNG) well-logging tool was run on a borehole at the Muskeg River Mine (MRM14 Cr0008) to acquire a continuous clay mineral and bitumen log. The extracted core was described in a subfacies context, but no additional mineralogical analysis was undertaken for this borehole.

Table 1
Analysis type and number, chronology and relationships between data, mine locations, and methods.

XRD	Phase 1 (a)	Phase 2 (a)	Phase 3 (b)
Bulk	31	188	67
CEC	31	0	67
Clays	31*	188*	67**
Elemental Analysis (XRF and INAA)			67
Detailed Mineral Identification by XRD			4***
SEM Imaging		12****	1*****
Light Microscopy			1
Natural Gamma-Ray Spectroscopy (NGS)			On cores, 10 cm spacing
Pulsed Neutron Generator well-logging			Muskeg River Mine (MRM14 Cr0008)

(a) Subfacies in Muskeg River Mine and Jackpine Mine (multiple locations).
(b) Cores from Muskeg River Mine (MRM13 Cr0101) and Jackpine Mine (JPM13 Cr3017).
*MIF.
**Profile Modeling.
***Muskeg River Mine (MRM13 Cr0101).
****Dispersion.
*****Cryogenic ultra-microtome.

3. Methods

3.1. X-ray diffraction (XRD)

3.1.1. Whole rock

Approximately 3 g of each sample, cleaned of bitumen if necessary by washing in toluene, was micronized in ethanol to nominally < 10 μm using a McCrone mill and the resulting slurry spray-dried directly from the mill [26,27,29]. X-ray powder diffraction (XRPD) patterns obtained from the spray dried specimens were recorded on either a Siemens D5000 using CoKα radiation with a scintillation point detector and scanning in 0.02° steps counting for 2 s per step between 2 and 75° 2θ or a Panalytical Xpert Pro with an Xcelerator position sensitive detector using CuKα radiation scanning in 0.0167° steps counting for 100 s per step between 3 and 70° 2θ. Quantitative mineralogical analysis of these patterns was made using a normalized reference intensity ratio (RIR) method based on optimized fitting of prior measured reference diffraction patterns for all minerals identified. The procedure is identical to that described in detail on pages 754–756 in Omotoso et al., [44]. Expanded uncertainty using a coverage factor of 2, i.e. 95% confidence, is estimated by $\pm X^{0.35}$, where X is the concentration in wt.%., e.g. 30 wt % ±3.3 [28].

3.1.2. Clay size fraction mineralogy

Analyses of the clay mineralogy of < 2 μm clay size fractions prepared as highly oriented specimens to enhance diffraction from 'basal' (00 l) clay mineral reflections were made in two different labs.

At the James Hutton Institute, a clay mineral analysis procedure was applied to fractions of <2 μm obtained by timed sedimentation according to Stokes' Law after mild crushing and ultrasonic dispersion. Oriented specimens of the <2 μm fractions so obtained were prepared by the filter peel transfer technique [39]. Some data were collected using the Siemens D5000 and some using the Panalytical Xpert Pro with scanning parameters as per whole rock data, except for limiting the range to 45° 2θ. In both cases patterns were recorded in the air-dried state, after ethylene glycol solvation, and after heating to 300 °C for one hour. Clay minerals identified were quantified using a mineral intensity factor (MIF) approach based on diffraction patterns calculated with the NEWMOD program (Hillier, 2003). The expandability (% smectite) in mixed-layer I-S was estimated based on comparison to calculated reflection migration data [39].

For samples from the cores from the Muskeg River Mine and the Jackpine Mine clay mineral analysis was performed at Qmineral BVBA. For these samples clay minerals were prepared by a methodology based on isolating clays following an extensive mechanical and chemical treatment [36]. Samples were first disaggregated by soaking, crushing, and ultrasonic agitation. Carbonates were removed by a sodium-acetate solution buffered to a pH of 5, and organic matter by a hydrogen peroxide treatment. A final sodium dithionite treatment was made to

remove Fe/Mn-(hydr)-oxides. Size fractions of <2 μm fraction were then separated by centrifugation according to Stokes' law, calcium saturated, washed free of chloride by dialysis and prepared as oriented specimens by sedimentation. Diffraction patterns were collected using CuKα radiation and step scanning from 2 to 47° 2θ in 0.05° steps counting for 2 s per step on a Philips PW1700. Specimens were acquired under air-dried conditions and then following ethylene glycol solvation. Selected samples were also prepared in Mg^{2+} and K^{+} saturated forms to assist in the discrimination between chlorite, smectite, and vermiculite by additionally recording diffraction patterns after heating to 350 °C and 600 °C. Patterns were modelled using the NEWMOD-2 program [39,38] with the same model parameters used to fit both air-dried and ethylene glycol treated specimens following the multi-specimen approach advocated by [49].

3.1.3. Cation exchange capacity (CEC)

CEC measurements were made using the cobalt hexamine trichloride method [9,13], initially developed for use on soils. The methylene blue method is more typically used in McMurray Formation characterization to illuminate the surface charge characteristics of clay surfaces. The method is based on adding a solution of known concentration of cobalt hexamine trichloride to the sample. The CEC is calculated by the difference between the initial cobalt complex concentration and the amount of cobalt complex remaining in solution. The cobalt complex concentrations are determined by spectrophotometry at a fixed wavelength of 480 nm where there is an assumed linearity between the concentration and the absorbance measured [9,13]. The exact method used in this study has been described in more detail by Gray et al. [22].

3.1.4. Transmitted light microscopy

A representative thin section was taken from the Muskeg River Mine core at an interval depth of 60.64–60.70 m. The sample comes from the lower McMurray Formation and the core description places the sample in a course-grained fluvial channel facies. The bitumen was removed from the sample with toluene washing and the resulting sample was impregnated with blue epoxy by TPS Enterprises, (Houston, Tx). A sodium cobaltinitrate stain was added to the thin section to aid potassium feldspar (yellow) identification.

3.1.5. Cryogenic-scanning electron microscopy (cryo-SEM)

Scanning electron microscopy under cryogenic conditions (cryo-SEM) was performed at Shell Technology Center, Amsterdam, to understand the *insitu* relationship between bitumen and the mineral matrix. The representative sample was taken from the Muskeg River Mine core at a core depth of 63.39–63.44 m (LM), in a coarse-grained fluvial channel facies. Standard bitumen and water content data report the sample to have previously contained 11.2% bitumen by soxhlet extraction, 7.2% water (due to core handling in sample preparation no pore water was observed in this study), and 81.2% solids. A center cut (approximately 5 mm by 5 mm) of the sample was prepared with a razor blade and glued to a sample holder using "Tissue-Tek", a cryo-SEM specific glue. The sample was frozen in 'slushy nitrogen' and kept in cryogenic conditions, below −90 °C, for the duration of further sample preparation and whilst imaging. The sample was imaged in a JEOL JSM-700F Field Emission SEM with a conductive platinum coating. A flat surface for imaging was prepared using an ultra-microtome under cryogenic conditions.

3.1.6. Elemental analysis:

X-ray fluorescence (XRF) for major element oxides was performed on subsets of the same 67 core samples from the Muskeg River Mine and Jackpine Mine cores used for mineral analysis. XRF was performed by Activation Laboratories, Ancastor, Canada, with lower limits of detection > 0.01 wt%. Prior to fusion, the loss on ignition (LOI), which includes H_2O^{+}, CO_2, S and other volatiles, was determined from the weight loss after thermally treating the sample at 1050 °C for 2 h. The fusion disk was made by mixing a 0.5 g of the thermally treated sample with 6.5 g of a combination of lithium metaborate and lithium tetraborate with lithium bromide as a releasing agent. Samples were analyzed on a Panalytical Axios Advanced wavelength dispersive XRF. Uranium and Thorium were determined in parts per million by Instrumental Neutron Activation Analysis (INAA). The lower limit of detection for Thorium is 0.2 ppm and 0.1 ppm for Uranium.

3.1.7. Natural Gamma-ray spectroscopy (NGS)

Natural Gamma-ray Spectroscopy (NGS) measurements on cores from the Muskeg River Mine [length 30.0–92.1 m] and Jackpine Mine [length 22.7–101.0 m], were acquired by Weatherford Laboratories in Houston, Texas. NGS spectra were acquired in a point-by-point mode using the standard NGS scanner. Spectral gamma-ray logging measures K, U, and Th and can be used to assess facies, stratigraphy, and provenance [43,14,21]. Point measurements were acquired every 10 cm for 300 s in the core to reduce artefacts in the acquired spectra by eliminating edge effects, errors from missing core sections, and transfer belt speeds. The detector is 75 mm in diameter and collimated using a lead shield, resulting in a spot size of ~10 cm. Due to low gamma-ray counts in core material from the McMurray Formation no other core boxes were present in the scanning room at the time of spectra acquisition and background spectra were measured three times per day for 1200 s.

Spectra processing was done in-house at Shell International Exploration and Production Inc. using proprietary codes. In brief, a background subtraction step was employed where the 1200 s background was normalized to the 300 s acquisition time and the background spectra were removed from all acquired spectra. Next the number of channels in background corrected spectra was reduced from 1024 channels to 256 channels. Finally, -the corrected spectra were converted into K, U and Th contributions to signal spectra measured using K, U and Th standards to obtain K, U and Th spectral yields [y] according to:

$$[y] = \left([S]^{T} * [S]\right)^{-1} * \left[[S]^{T} * [s]\right)^{-1}$$

where [S] is the matrix of K, U and Th signal spectra and [s] is the acquired spectra corrected for background.

K, U and Th yields were then validated against the XRF and neutron activation measurements to produce a calibrated synthetic log.

Unlike the laboratory core measurements, downhole NGS as part of the field trial has far fewer issues with background effects. In the field trial of a slim-hole well-logging tool (see next section) run in core hole MRM14 Cr0008 from the Muskeg River Mine the gamma-ray detector in the tool is fully surrounded by the formation so background effects are negated. Signal to noise issues due to limited time of signal acquisition can be overcome with appropriately slow logging speeds. Logging speeds in this study were 30 m/hr.

3.1.8. Pulsed neutron generator well-logging tool field trial

A pulsed neutron generator (PNG) two gamma-ray detectors slim-hole tool was run in core hole MRM14 Cr0008. This slim-hole PNG tool from Halliburton (RMT^{TM}i) allowed the measurement of neutron induced gamma-ray spectra with a vertical resolution of approximately 10 cm. PNG based well-logging tools are an active area of research and development (e.g. [52,10,34] and references therein; [51,53]). The RMT™i tool was used for its slim-hole design compatible with the core hole diameter.

PNG emits 14 MeV neutrons produced in a fusion reaction which interact with atom nuclei in the formation. Inelastic and capture reactions within the nuclei of different elements cause the emission of gamma-rays with different energies which are measured by a gamma-ray spectrometer. The measured gamma-ray signal is proportional to the convolution of the neutron flux distribution, the elemental concentration distribution, and the distribution of the density (related to gamma-ray scattering). The RMT™i tool uses a high-density bismuth germanium oxide detector and captures the inelastic spectra of carbon

between 4.1 and 4.4 MeV. The downhole logging speeds were 30 m per hour over two loggings runs in which passive and active PNG modes were used to capture initially K, U, and Th yields and finally inelastic spectra of carbon. This paper omits the analysis of all other inelastic and capture elements as these are beyond scope and intent of this paper.

4. Results

4.1. Bulk mineralogy and cation exchange capacity

The mineralogy analyses samples lower, middle, and upper McMurray Formation sediments with subfacies that comprise, in no particular order, marsh, distributary channels, flood plain/overbank, back swamp, fluvial channels (coarse and fine) estuarine channels, tidal flats, mixed tidal flats, middle shoreface, and upper shoreface. The mineralogy is dominated by quartz with clay minerals making up most of the remaining mineral suite (Fig. 3 and see Supplemental data for all bulk analyses). Minerals identified by whole rock XRD are quartz, plagioclase, K-feldspar, calcite, dolomite, siderite, anatase, and pyrite. Both K-feldspar and plagioclase are present; K-feldspar tends to be more common. Traces of calcite and dolomite are present in many samples, but minor siderite is the main carbonate identified and in one sample exceeds 50% where a siderite nodule readily identified in core was sampled. Illite and mixed-layer illite–smectite dominate the 2:1 clays. Kaolinite is abundant is many samples. In most samples, kaolinite appears to be a poorly crystalline variety, characterized by broad basal reflection widths typically indicative of small crystallite size. Additionally, a kaolinite-expandable mixed-layer mineral (using the terminology recommended by Hughes et al. [33] is present in some samples. The exact kaolinite mixed-layering type is not clear from the random powder whole rock XRD patterns, but the presence of the mineral is signaled by diffraction features indicative of a kaolinite-like mineral but with extremely weak basal reflections, relative to non-basal bands, and an 06,33-band position that indicates a larger unit cell b-dimension compared to kaolinite (Fig. 4). Insert ('a') of the detail of the 02,11 diffraction band shows the largely turbostratic nature of the clay minerals in the back swamp subfacies sample (lower pattern) compared to tidal channel (upper pattern) where non-basal peaks due to kaolinite are evident in the tail of the 02,11 band (Fig. 4). Note also the 06,33 band which appears to be a doublet in the tidal channel sample with a component that can attributed to kaolinite (1.488 Å) but is broadened and shifted to larger d-spacing (1.495 Å) in the back-swamp sample i.e. a position that is intermediate between kaolinite and montmorillonite. The oriented clay size fraction traces (insert 'b') show the relatively unresponsive clays in the tidal channel sample compared to the clays in the back swamp sample where kaolinite/expandable and vermiculitic clays are evident from the various responses and changes between air-dried, ethylene glycol solvated and heated XRD traces.

The full pattern method for bulk sample mineral quantification used in this study allows the repeated identification and quantification of this mineral by the inclusion of a kaolinite-smectite standard with similar diffraction characteristics obtained from the Jurassic Blisworth Clay of Northamptonshire, England [29,27]. In several samples, the kaolinite-expandable mixed-layer clay is the most abundant clay mineral in the sample accounting for around 60% by weight.

Cation exchange capacity varies from very low < 1 cmol(+)kg^{-1} to as high as 45 cmol(+)kg^{-1}. Broadly speaking CEC tracks with total clay content (Fig. 3) and as might be anticipated from this relationship CEC is generally higher in the muddier facies. Facies described as marsh, coal swamp, back swamp and flood plain/overbank tend to have elevated CECs.

On a stratigraphic basis, the middle McMurray Formation tends to have the simplest mineralogy (Fig. 4) with quartz dominating the system and two clay minerals, kaolinite and illite–smectite, making up most of the mineral assemblage. The CEC is low, and this suggests that the expandability of the illite–smectite (% smectite layers) in the middle McMurray formation is also low, a feature which is confirmed by more detailed clay fraction XRD analysis, see below. The upper McMurray Formation has more clay minerals and the ratio between illite–smectite and kaolinite changes in favour of illite–smectite and the CEC suggests a more expandable form of illite–smectite, which is again confirmed by more detailed clay fraction analyses, see below. Features observed in core suggest (Fig. 2) that the sand to clay ratio decreases because it is heavily influenced by the draping of muddier zones over the shoreface sands during times of lower energy.

The lower McMurray Formation is the most complex zone in terms of mineralogy. Where coarse fluvial channels have migrated across the depositional system the mineralogy is dominated by quartz, with minor

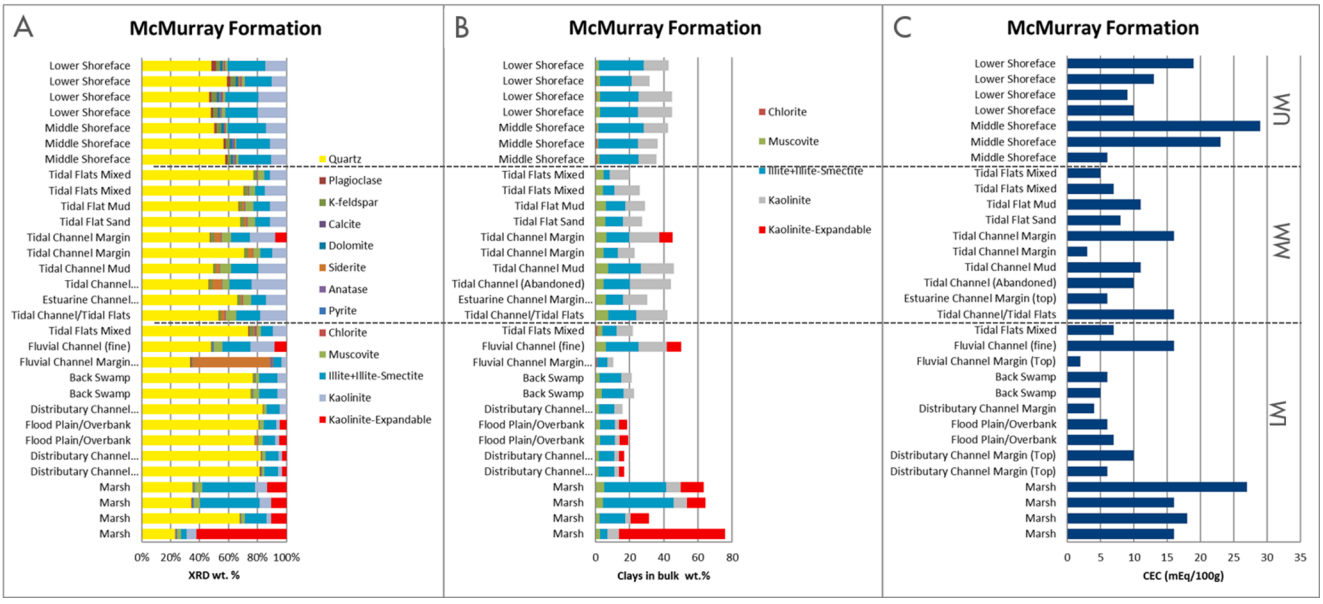

Fig. 3. Bulk mineralogy (31 samples) covering all facies and mineral types from the Muskeg River Mine and Jackpine mine (A), clay minerals in the bulk analysis (B) and (C) cation exchange capacity (CEC). Samples are in their subfacies order and their position in the stratigraphy lower McMurray (LM), middle McMurray (MM) or upper McMurray (UM).

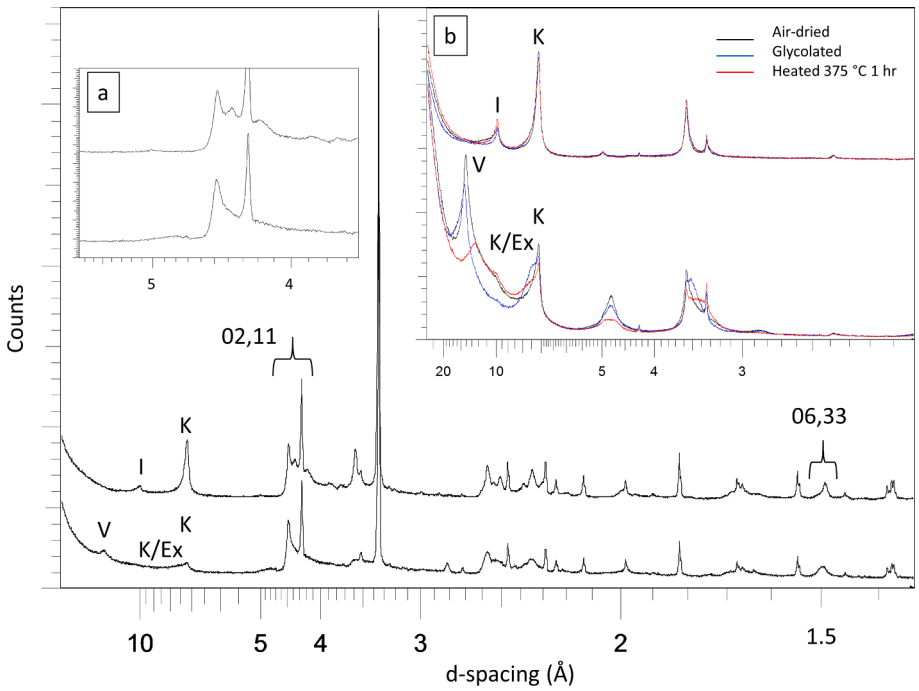

Fig. 4. XRD patterns of contrasting clay rich samples from the McMurray Formation. Main patterns are random power whole rock XRD patterns, insert 'a' shows close up of the 02,11 diffraction band, and insert 'b' shows oriented clay size fractions (<2 μm) from the same two samples. Lower patterns are from a back swamp subfacies in the McMurray Formation (LM) and upper patterns are from a tidal channel in the middle McMurray Formation. Both samples contain similar amounts of clay. K = kaolinite, K/Ex = kaolinite-expandable mixed-layer, I = illitic clays (illite plus mixed-layer illite/smectite), V = vermiculitic clays. Note most of the sharp peaks in the random powder whole rock XRD patterns are due to quartz.

feldspar and kaolinite. Where the depositional energy was lower kaolinite is more prevalent with significant amounts of kaolinite-expandable mixed-layer mineral found in sediments assigned to marsh facies. Other subfacies such as back swamp or coal swamp environments presumably also had conditions conducive to soil formation, though paleosols are not normally identified as such in the facies nomenclature. The mixed-layering of the clays in these facies gives rise to a CEC response that can be quite high $\sim 20\,\mathrm{cmol} + \mathrm{kg}^{-1}$. Whereas, the CEC response in the channel sands is low and associated with only a minor illite–smectite component whose expandability is also low.

The bulk mineralogy on the cores from the Muskeg River Mine and Jackpine Mine (cores MRM13 Cr0101 and JPM13 Cr3017, respectively) adhere closely to the scheme laid out above. The cores illuminate the fact that the lower McMurray Formation may be variable in thickness as the Jackpine Mine core has little Lower McMurray Formation whereas the Muskeg River Mine core has a thick lower McMurray Formation section with virtually no cation exchange response. The Muskeg River Mine core also has a sample that is somewhat unique within the whole sample set. Its CEC is 44.6 $\mathrm{cmol} + \mathrm{kg}^{-1}$ and the mineral assemblage is dominated by kaolinite and kaolinite-expandable mixed-layer mineral. At its base, the Jackpine Mine core has a similar mineral assemblage in the marsh subfacies but with less pronounced character and CEC response. Given the subfacies nomenclature and the expandable nature of the kaolinite, clays in this zone most likely represents a paleosol, although no detailed paleosol analysis (e.g. palynology) is undertaken here.

4.2. Clay size fraction (<2 μm) mineralogy

Four clay mineral phases were identified, namely, discrete illite, discrete kaolinite and two mixed-layered minerals, illite–smectite and kaolinite-expandable mixed-layer. Illite-smectite tends to be the most abundant clay mineral present but in a few samples, kaolinite is of greater or subequal abundance, whilst the kaolinite-expandable mixed-layer mineral is confined to certain subfacies. Two types of mixed-layer illite-smectite were identified. One is a random mixed-layer illite-smectite, with ≈60–70% expandability (smectite layers). This type only occurs in upper McMurray Formation samples and some marsh subfacies within the lower McMurray Formation. This distribution is consistent with the CEC measurements on the bulk samples. Most other samples have a mixed-layer illite-smectite with ≈20–30% expandability (with R1 ordering) which is presumably reflective of the source terrain. The kaolinite-expandable mixed-layer mineral was identified in the clay fraction of many samples, most often in marsh subfacies or other low energy facies of the lower McMurray Formation or in middle McMurray facies with a fine-grained nature. Many of these samples also show a reflection at around 14.2 Å, that is quite intense and sensitive to heating, suggesting a vermiculite-like character (Fig. 5). Interestingly, the vermiculitic behavior is most obvious in samples that also contain obvious kaolinite-expandable mixed-layer mineral. Thus, such samples exhibit a series of reflections that are conceptually suggestive of mixed-layering between 7 Å (kaolin) and 14 Å (vermiculite) expandable components, although the main certainty is a close association of a kaolinite-expandable mixed-layer mineral and a vermiculitic phase. A more detailed analysis follows later but it can be considered that "kaolinite-vermiculite" may be a more apt description of the kaolinite-expandable mixed-layer mineral in many samples. Additionally, some samples show a reflection which upon heating show behaviors more consistent with chlorite, and it is possible that such samples may contain trace/minor chlorite. In general, it is also noteworthy that when identified in the whole rock samples the kaolinite-expandable mixed-layer mineral is a dominant component in the <2 μm clay fraction separates.

Samples from the cores from the Muskeg River Mine and Jackpine Mine gathered for the NGS data analysis campaign were scrutinized in detail (Tables 2 and 3 and Supplemental data) using modelling of the 1D diffraction pattern of the <2 μm fractions. Illite and kaolinite were modelled with relatively small crystallite size distributions with the number of layers in the coherent scattering domain (N) between 8 and 15 for illite and 14–29 for kaolinite. Chlorite, if present, required small crystallite sizes, N < 10. Mixed-layer minerals were modelled as kaolinite-smectite, illite–smectite, and a complex hydroxy interlayered mineral (HI-mineral). Kaolinite-smectite was randomly interstratified with proportions 82:12. Two varieties were modelled with different N values 2–5 and 2–10, respectively. The illite-smectites, identified previously, were confirmed in terms of their subfacies and formation associations and ranges of expandability. The most expandable illite–smectite identified was randomly interstratified usually with around 80% expandable layers and found mainly in shoreface sands of

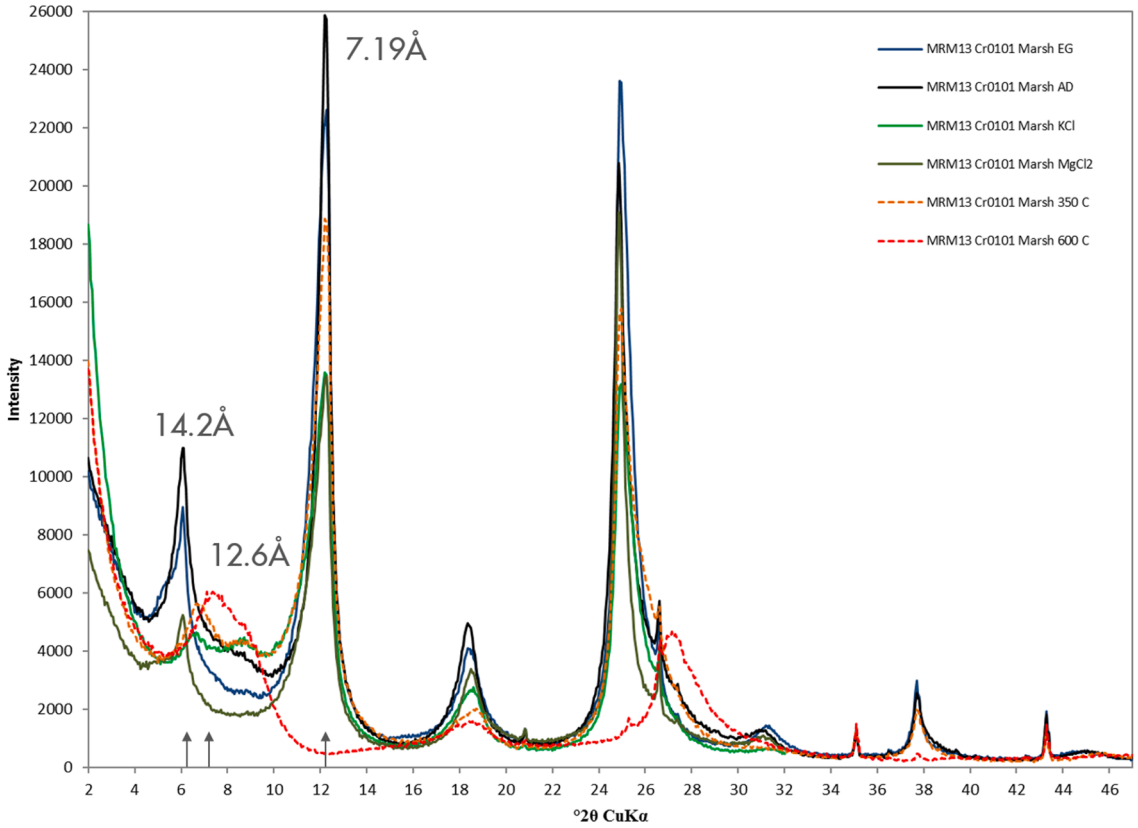

Fig. 5. Detailed phase identification in marsh facies sample from Muskeg River Mine core. Initial patterns were acquired in air-dried (AD) and ethylene glycolated (EG) states. Following Mg-saturation and ethylene glycol solvation the 14.2 Å peak did not migrate. K-saturation resulted in collapse of most of the 14.2 Å peak to a broad ~ 10.0 Å peak. Heating of the K-saturated sample to 350° C and 600° C created degradation of the 14.2 Å and 7.19 Å peaks at 600° C leaving a very broad composite peak with at least two maxima scattering between these positions. The behavior of 14.2 Å peak indicates vermiculitic character. Arrows mark the d-spacings given on the figure.

the upper McMurray Formation. The other subfacies and Members contained a much less expandable form usually around 20% expandable. The lower expandable variety of illite–smectite was also found to have a wide crystallite size distribution. The clay minerals modelled as HI-minerals are confined to marsh subfacies samples and are expressed as a complex reflection around 14.2 Å, and clearly correspond to the clay identified as some form of vermiculite in the earlier phase of the investigation.

To better understand the nature of the expandable clay mineral in sediments in the marsh subfacies a series of cation saturation steps were used (Fig. 5). The original sample with CEC of 45 cmol(+)kg^{-1} from the Muskeg River Mine core was Mg-saturated and subjected to a glycerol solvation to test for smectite. Should the 14.2 Å reflection be related to smectite it would migrate to ≈17 Å. Since, it was stable under Mg-saturation and glycerol solvation, a smectitic character was ruled out. To understand the mineralogy further, a chlorite test was performed in which the sample was K-saturated. A shift to a broad reflection around 10 Å confirms that the 14.2 Å reflection is related to a vermiculitic mineral, presumably discrete and free from kaolinite interstratification. Heating to 350 °C has a minor effect on the 14.2 Å reflection and little effect on the 7.19 Å reflection. Heating to 600 °C significantly degrades the 7.19 Å reflection and collapses the 14.2 Å reflection to a very broad reflection with two maxima at 12.6 Å and 10.1 Å with significant intensity distributed towards both lower and higher d-spacings. Whether these peak shifts reflect the degradation of a mixed-layer mineral, or the separation of associated discrete phases is a point of conjecture. These heat treatments also suggest there may be an element of hydroxy interlayering in the vermiculitic mineral, although the behavior observed can also be indicative of relatively high layer charge. In this context, the vermiculite character is consistent with the elevated CEC values recorded on the whole rock material from marsh subfacies. While the sample from the Muskeg River Mine core is the most obvious marsh subfacies the Jackpine Mine core also has marsh subfacies that when qualitatively compared have some remarkable similarities (Table 2).

4.3. Imaging

The large channels in the lower McMurray Formation are composed of coarse clastic material (1–2 mm grain diameter). A sample was imaged using transmitted light microscopy (Fig. 6) and is dominated by quartz grains (white). Blue areas are epoxy impregnated and may be considered porosity that was either water or bitumen filled prior to drying and bitumen extraction. Grains, approximately the same size as quartz, appearing with a yellowish colour are K-feldspar. Some K-feldspars have a greenish tint which is indicative of their alteration to kaolinite. Opaque areas are small isolated patches of non-extracted bitumen. Quartz is the dominant mineral and varies in particle size. Kaolinite is observed as a complete or partial replacement of K-Feldspar. Note that quartz grains have clay coats that vary in thickness and continuity, but their positive identification is below the resolution of the transmitted light images. No point count data were generated for this sample but qualitatively the petrology reported by Hein et al. [24] where quartz dominates the channel facies of the McMurray Formation may be used as a reference.

Cryo-SEM imaging reveals that where bitumen has been plucked from the quartz, clay minerals are adhered to the quartz surface (Fig. 6). In some cases, the positive identification of kaolinite based on morphology can be made and where the contact between bitumen and

Table 2
Modelled <2 μm clay mineralogy for Muskeg River Mine (32 samples) and Jackpine Mine (28 samples). Seven samples did not yield sufficient material for pattern modeling. Discrete and mixed-layer minerals were quantified. Illite-smectite is quantified to have both a high and low expandable component that is facies segregated. Higher expandable I-S is predominantly found in the upper McMurray Formation. Four samples have vermiculite and complex hydroxy-interlayered minerals. (*) Average Size of the coherently scattering domains in the c* direction, expressed as a number of layers. (**) Per full unit cell. (***) These are mixed layers composed of Illitic layers, Expandable layers and hydroxyl-interlayers (HI-minerals).

				Mineral	**Illite**							*Kaolinite*							Chlorite		*Vermiculite*	KS	**IS**																HI-minerals	SUM
				Reichweite																		KS (R0)	**IS (R0)**				**IS(R1)**													IExpHIexp (***)	
				Proportions																		0 82:	**0 10:**	**0 20:**	**0 22:**	**0 22:**	**1 67:**	**1 72:**	**1 72:28**	**1 75:**	**1 77:**	**1 78:**	**1 78:**	**1 78:**	**1 78:**	**1 78:**	**1 81:**	**1 81:**	20:40:40	
				N (*)																		18	**90**	**80**	**78**	**78**	**33**	**28**		**25**	**23**	**22**	**22**	**22**	**22**	**22**	**19**	**19**	(***)	
Facies	Mine	Core and Depth (m)	Fraction analyzed	Fe-content (**)	**8 0**	**9 0**	**11 0**	**12.5 0**	**13 0**	**14 0**	**15 0**	*14*	*15*	*17*	*19*	*21.5*	*24*	*25*	*29*	8	8.5	10		5	10	**4 0.20**	**3.5 0.25**	**3.5 0.38**	**4 0.38**	**10 0.3**	**2 0.2**	**10 0.3**	**2 0.2**	**3 0.2**	**1 0.2**	**2 0.2**	**2 0.25**	**2 0.15**	**2 0.2**	**2 0.25**	**2 0.36**	7 0.2	
Lower Shore face	MRM13	Cr0101 4.34 to 4.425 m	<2 μm							**20**								*76*													**4**									100
Lower Shore face	MRM13	Cr0101 11.815 to 11.865 m	<2 μm					**36**										*37*		3		8									**16**									100
Lower Shore face	MRM13	Cr0101 12.6 to 12.655 m	<2 μm					**36**										*36*		4		8									**16**									100
Tidal Mud Flat	MRM13	Cr0101 16.135 to 16.19 m	<2 μm					**29**										*27*		1		11										**32**								100
Tidal Mud Flat	MRM13	Cr0101 18.06 to 18.11 m	<2 μm					**36**										*32*		1		11									**20**									100
Tidal Mud Flat	MRM13	Cr0101 20.77 to 20.825 m	<2 μm					**41**										*35*		1		8									**15**									100
Tidal Mud Flat	MRM13	Cr0101 23.615 to 23.67 m	<2 μm					**33**										*29*				15									**23**									100
Tidal Flat Mixed	MRM13	Cr0101 28.18 to 28.235 m	<2 μm	**37**										*17*						2		17									**27**									100
Tidal Flat Mixed	MRM13	Cr0101 30.03 to 30.085 m	<2 μm			**45**								*34*						1		8									**12**									100
Tidal Flat Mixed	MRM13	Cr0101 32.61 to 32.665 m	<2 μm		**36**								*25*									15									**24**									100
Tidal Mud Flat	MRM13	Cr0101 36.25 to 36.3 m	<2 μm		**34**									*25*						0.5			14													**27**				101
Tidal Mud Flat	MRM13	Cr0101 36.465 to 36.515 m	<2 μm		**32**									*15*									15													**38**				100
Tidal Mud Flat	MRM13	Cr0101 39.135 to 39.185 m	<2 μm		**32**									*21*									14														**33**			100
Tidal Mud Flat	MRM13	Cr0101 43.345 to 43.4 m	<2 μm		**33**									*17*									16														**34**			100

(*continued on next page*)

Table 2 (*continued*)

Facies	Mine	Core and Depth (m)	Fraction analyzed	Mineral	**Illite**							*Kaolinite*							Chlorite		*Vermiculite*	KS		**IS**																HI-minerals	SUM
				Reichweite																		KS (R0)		**IS (R0)**				**IS(R1)**														IExpHIexp (***)	
				Proportions																		0	0	**0**	**0**	**0**	**0**	**1**	**1**	**1**	**1**	**1**	**1**	**1**	**1**	**1**	**1**	**1**	**1**	**1**		
				N (*)																		82:	82:	**10:90**	**20:80**	**22:78**	**22:78**	**67:33**	**72:28**	**72:28**	**75:25**	**77:23**	**78:22**	**78:22**	**78:22**	**78:22**	**78:22**	**78:22**	**81:19**	**81:19**	20:40:40 (***)	
				Fe-content (**)	**80**	**90**	**110**	**12.50**	**130**	**140**	**150**	*14*	*15*	*17*	*19*	*21.5*	*24*	*25*	*29*	8	8.5	10	5	10	**4**	**3.5**	**3.5**	**4**	**10**	**10**	**10**	**10**	**10**	**9**	**9**	**9.5**	**10**	**9.5**	**9.5**	7	0.2
																								0.20	**0.25**	**0.38**	**0.38**	**0.3**	**0.2**	**0.3**	**0.2**	**0.2**	**0.1**	**0.2**	**0.25**	**0.15**	**0.2**	**0.25**	**0.36**		
Marsh	MRM13	Cr0101 45.52 to 45.58 m	<2 μm									*47*									*2*		21		**1**															29	100
Marsh	MRM13	Cr0101 50.42 to 50.475 m	<2 μm			**30**									*36*								13																	**21**		100
Fluvial Channel Margin	MRM13	Cr0101 53.49 to 53.545 m	<2 μm						**26**						*72*																									**2**		100
Fluvial Channel Top	MRM13	Cr0101 54.13 to 54.19 m	<2 μm						**17**						*81*																									**2**		100
Fluvial Channel Top	MRM13	Cr0101 54.345 to 54.395 m	<2 μm						**12**						*87*																									**1**		100
Fluvial Channel Coarse	MRM13	Cr0101 56.385 to 56.44 m	<2 μm			**15**							*84*																								**1**				100
Fluvial Channel Fine	MRM13	Cr0101 57.08 to 57.13 m	<2 μm			**34**								*51*									6														**9**				100
Fluvial Channel Breccia	MRM13	Cr0101 57.23 to 57.28 m	<2 μm			**27**									*52*								7														**14**				100
Fluvial Channel Coarse	MRM13	Cr0101 59.47 to 59.52 m	<2 μm			**20**									*73*								1														**6**				100
Fluvial Channel Fine	MRM13	Cr0101 60.64 to 60.7 m	<2 μm			**9**								*91*																												100
Fluvial Channel Coarse	MRM13	Cr0101 64.115 to 64.19 m	<2 μm			**10**								*90*																												100
Fluvial Channel Fine	MRM13	Cr0101 67.045 to 67.1 m	<2 μm			**8**								*92*																												100
Fluvial Channel Margin	MRM13	Cr0101 69.4 to 69.46 m	<2 μm			**32**								*51*									8														**9**				100
Fluvial Channel Coarse	MRM13	Cr0101 72.105 to 72.16 m	<2 μm			**21**								*77*																								**2**				100
Fluvial Channel Coarse	MRM13	Cr0101 76.695 to 76.75 m	<2 μm			**8**									*92*																												100
	MRM13		<2 μm			**5**													*95*																								100

(*continued on next page*)

Table 2 (*continued*)

Facies	Mine	Core and Depth (m)	Fraction analyzed	Mineral	**Illite**							*Kaolinite*							Chlorite			*Vermiculite*	KS	**IS**																		HI-minerals	SUM
				Reichweite																			KS (R0)	**IS (R0)**					**IS(R1)**															IExpHIexp (***)	
				Proportions N (*)																			0 82: 18	0 **10: 90**	**20: 80**	**22: 78**	**22: 78**	**67: 33**	**72: 28**	1	**75: 25**	**77: 23**	**78: 22**	**78: 22**	**78: 22**	**78: 22**	**78: 22**	**81: 19**	**81: 19**	20:40:40 (***)	
				Fe-content (**)	**80**	**90**	**110**	**12.50**	**130**	**140**	**150**	*14*	*15*	*17*	*19*	*21.5*	*24*	*25*	*29*	8	8.5	10		5	10	**4 0.20**	**3.5 0.25**	**3.5 0.38**	**4 0.38**	**10 0.3**	**10 0.2**	**10 0.3**	**10 0.2**	**10 0.2**	**9 0.1**	**9 0.2**	**9 0.25**	**9.5 0.15**	**10 0.2**	**9.5 0.25**	**9.5 0.36**	7 0.2	
Fluvial Channel Coarse		Cr0101 79.29 to 79.34 m																																								
Fluvial Channel Coarse	MRM13	Cr0101 79.66 to 79.715 m	<2 μm			**7**												*93*																									100
Fluvial Channel Coarse	MRM13	Cr0101 80.74 to 80.78 m	<2 μm			**7**												*93*																									100
Upper shoreface	JPM13	Cr3017 23.775 to 23.87 m	<2 μm							**26**								*36*	5				1		**15**																	**17**		100
Upper shoreface	JPM13	Cr3017 23.955 to 24.005 m	<2 μm							**27**								*27*	5				3		**13**																	**25**		100
Upper shoreface	JPM13	Cr3017 24.095 to 24.15 m	<2 μm							**30**								*27*	5				3		**15**																	**20**		100
Upper shoreface	JPM13	Cr3017 25.68 to 25.735 m	<2 μm							**31**								*27*	4				1		**15**																	**22**		100
Upper shoreface	JPM13	Cr3017 25.88 to 25.935 m	<2 μm							**27**								*34*	4				2		**8**																	**25**		100
Upper shoreface	JPM13	Cr3017 25.885 to 25.94 m	<2 μm							**22**								*21*	3				3			**32**				**19**													100
Middle Shoreface	JPM13	Cr3017 26.17 to 26.225 m	<2 μm							**23**								*15*	3				3			**33**					**23**												100
Upper shoreface	JPM13	Cr3017 28.365 to 28.42 m	<2 μm							**25**								*17*	3				3			**34**					**18**												100
Upper shoreface	JPM13	Cr3017 28.48 to 28.535 m	<2 μm							**18**								*14*	3				4			**38**					**23**												100
Upper shoreface	JPM13	Cr3017 28.57 to 28.625 m	<2 μm							**17**								*10*	2				4			**45**					**22**												100
Middle Shoreface	JPM13	Cr3017 30.835 to 30.89 m	<2 μm							**24**								*25*	3				2				**27**				**19**												100
Tidal Flat Mixed	JPM13	Cr3017 35.96 to 36.015 m	<2 μm							**23**							*13*		1				8	**19**					**36**														100
Salt Marsh	JPM13		<2 μm							**24**						*15*			1				3	**31**				**26**															100

(*continued on next page*)

Table 2 (*continued*)

Facies	Mine	Core and Depth (m)	Fraction analyzed	Mineral	**Illite**							*Kaolinite*							Chlorite	*Vermiculite*	KS	**IS**															HI-minerals	SUM
				Reichweite																	KS (R0)	**IS (R0)**				**IS(R1)**											IExpHIexp (***)	
				Proportions																	0 82: 18	0 **10: 90**	**0 20: 80**	**0 22: 78**	**0 22: 78**	**1 67: 33**	**1 72: 28**	**1 75: 25**	**1 77: 23**	**1 78: 22**	**1 78: 22**	**1 78: 22**	**1 78: 22**	**1 78: 22**	**1 81: 19**	**1 81: 19**	20:40:40 (***)	
				N (*)																	82: 18																7	
				Fe-content (**)	**8 0**	**9 0**	**11 0**	**12.5 0**	**13 0**	**14 0**	**15 0**	*14*	*15*	*17*	*19*	*21.5*	*24*	*25*	*29*	8	8.5	10	5	10	**4 0.20**	**3.5 0.25**	**3.5 0.38**	**4 0.38**	**10 0.3**	**2 0.3**	**10 0.3**	**2 0.2**	**2 0.2**	**1 0.2**	**2 0.2**	**9 0.25**	**9 0.15**	**10 0.2**	**9.5 0.25**	**9.5 0.36**	0.2	
		Cr3017 41.115 to 41.17 m																																					
Tidal Channel/ Tidal Flat	JPM13	Cr3017 50.685 to 50.74 m	<2 μm							**26**							*62*			1		8					**3**											100
Tidal Channel/ Tidal Flat	JPM13	Cr3017 52.925 to 52.98 m	<2 μm							**26**							*26*			1		13	**2**				**32**											100
Tidal Mud Flat	JPM13	Cr3017 59.91 to 59.965 m	<2 μm		**26**												*8*			1		16	**1**				**48**											100
Tidal Channel/ Tidal Flat	JPM13	Cr3017 65.395 to 65.45 m	<2 μm		**25**												*9*			1		20					**45**											100
Estuarine Channel Fine	JPM13	Cr3017 71.61 to 71.66 m	<2 μm		**27**												*9*			1		18	**0.5**				**45**											101
Estuarine Channel Fine	JPM13	Cr3017 71.85 to 71.9 m	<2 μm		**27**												*17*			0.5		22					**34**											101
Estuarine Channel Top	JPM13	Cr3017 71.96 to 72.02 m	<2 μm						**24**								*49*			1		13						**13**										100
Estuarine Channel Fine	JPM13	Cr3017 74.115 to 74.165 m	<2 μm						**19**								*16*			1		18						**46**										100
Estuarine Channel Coarse	JPM13	Cr3017 76.105 to 76.16 m	<2 μm						**22**								*13*			1		17						**47**										100
Tidal Flat Sand	JPM13	Cr3017 78.44 to 78.5 m	<2 μm						**20**			*71*								0.5		2						**6**										100
Tidal Flat Sand	JPM13	Cr3017 80.02 to 80.07 m	<2 μm								**19**	*79*								1								**1**										100
Estuarine Channel Fine	JPM13	Cr3017 80.935 to 80.985 m	<2 μm								**5**	*94*																**1**										100
Marsh	JPM13	Cr3017 86.86 to 86.915 m	<2 μm								**18**		*8*						*2*			20						**29**									23	100
Marsh	JPM13	Cr3017 87.265 to 87.32 m	<2 μm								**12**		*4*						*2*			23						**42**									17	100
Marsh	JPM13		<2 μm								**12**		*3*						*2*			22						**43**									18	100

(*continued on next page*)

Table 2 (*continued*)

Facies	Mine	Core and Depth (m)	Fraction analyzed	Mineral Reichweite Proportions N (*)	Fe-content (**)	Illite				Kaolinite						Chlorite	Vermiculite	KS (R0)	IS (R0)				IS(R1)													HI-minerals SUM IExpHIexp (***)
		Cr3017 87.725 to 87.78 m				8	9	11	12.5	13	14	15	*14*	*15*	*17*	*19*	*21.5*	*24*	*25*	*29*	8	8.5	10	0	82: 18	10: 90	20: 80	22: 78	22: 78	67: 33	72: 28	72: 28	75: 25	77: 23	78: 22	78: 22	78: 22	78: 22	78: 22	78: 22	78: 81: 19	81: 19	20:40:40 (***)
					0.20	0.25	0.38	0.38	0.3	0.2	0.3	0.2	0.2	0.1	0.2	0.25	0.15	0.2	0.25	0.36	0.2

Table 3
Clay mineralogy reported in relative weight percent of the less than two micrometer fraction for patterns shown in Fig. 5. CEC is on the whole rock and tracks with vermiculitic phases. Elemental data is on the less than two micrometer weight fraction. Whole rock analysis is reported as weight percent.

	MRM13 Cr0101 Marsh 41.1 m	MRM13 Cr0101 Marsh	MRM13 Cr0101 Marsh 47.5 m	MRM13 Cr0101 Marsh 48.1 m
Illite (rel. wt.%)	16	0	14	0
ISS R1(rel. wt. %)	26	0	16	7
Kaolinite (rel. wt.%)	43	42	42	21
Kaolinite-Vermiculite (rel. wt.%)	12	30	23	53
HI-Minerals (rel. wt.%)	3	24.5	4	14
Vermiculite (rel. wt.%)	0	2.5	1	2
Smectite (rel. w. t%)	0	1	0	3
CEC from bulk (mEq/100g)	11.2	44.6	11.6	35.3
K_2O (rel. wt.%)	2.8	0.61	2.4	0.54
Th (ppm)	17.3	18.3	17.5	16.4
U (ppm)	3	0.5	2.5	3.9
Quartz (wt.%)	26.3	32.8	28.5	33.7
K-feldspar (wt. %)	1.3	2.5	1.1	2.3
Dolomite (wt.%)	0.4	0	0.2	0
Anatase (wt.%)	0.5	1.1	0.6	0.6
Pyrite (wt.%)	0	0.1	0	0
Mica (wt.%)	3.6	0.6	3.4	0
Kaolinite (wt.%)	38.5	40.2	32.2	15.5
Kaolinite-EXP ML (wt.%)	9.5	21.6	16.5	48
Illite + illite-smectite (wt. %)	19.9	1	17.6	0

4.6. Pulsed neutron generator field trial

A field trial during the annual mine coring program was performed at the Muskeg River Mine core (MRM14 Cr0008) and was logged with the RMT™i PNG tool in two modes. First, in passive mode recording only natural gamma-ray counts (K, U, and Th) and then in active mode capturing the inelastic spectra of carbon. The core was described by mine geologists following the facies convention adopted for the Muskeg River Mine, and basic water, bitumen, and solids contents were analysed as part of the regular coring program. The field trial generated K, U, and Th yields from the NGS logging trip were assigned their position within the described stratigraphy (Fig. 9). As with the laboratory results from core, NGS measurements on marsh subfacies in the Lower McMurray Formation (LM2) have elevated U*Th response. A gradient of 50X (where X is potassium yield multiplied by 1000) was used to generate the facies indicator (Fig. 9a), this gradient differs from that used in core scanning and is reflective of the difference between the background in borehole and core store/lab environment. For use in another mine this cut off should be locally calibrated.

The carbon yield calculated from the inelastic spectrum for carbon may be used as a proxy for bitumen content. As part of the standard core handling and analysis program within the core program routine Dean-Stark oil saturations by distillation extraction are measured down the length of any core retrieved from the subsurface. Water is vaporized by boiling toluene, condensed and collected in a calibrated trap. The solvent is condensed and flows back over the sample to extract oil. Sample weight is measured before and after extraction and oil volumes are then calculated from weight loss minus the weight of water in the original sample. As a result, simple linear correlations between carbon yield and bitumen concentration can be generated (Fig. 9b, c), putting aside any non-extractable bitumen phases. These correlations allow a continuous bitumen profile to be generated from the PNG tool and this can be combined with a facies indicator (Fig. 10). Ore grade bitumen contents need to be above 7 wt% bitumen to be considered economic for plant processing and a calculated bitumen profile through the MRM14 Cr0008 core hole highlights predominantly ore grade material in the lower

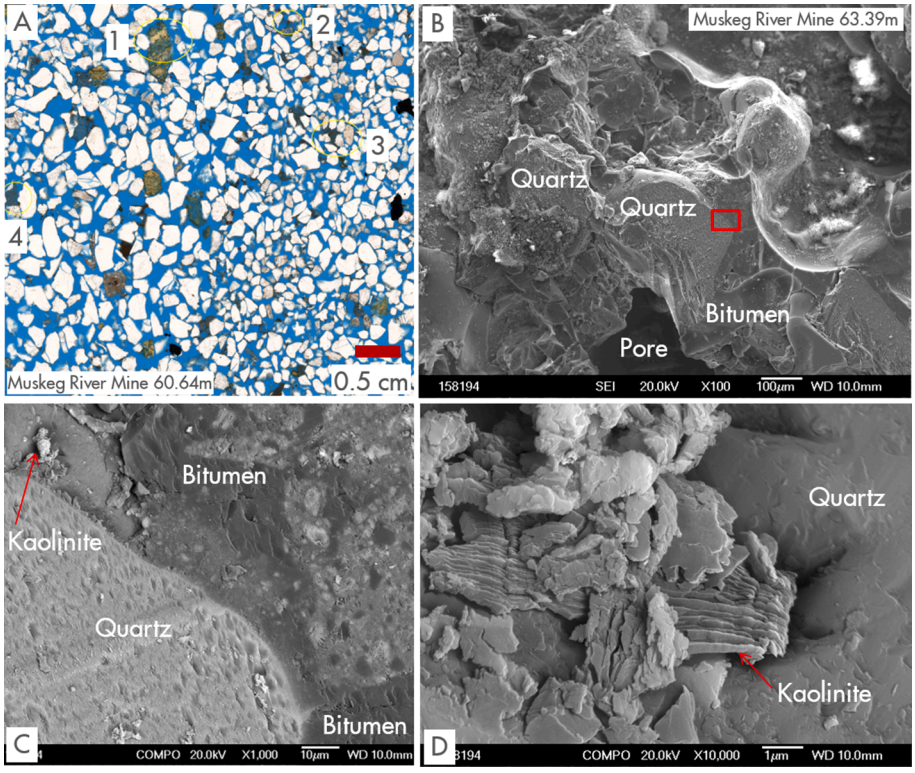

Fig. 6. A) Blue epoxy impregnated transmitted light thin-section image after bitumen extraction. Sample from a coarse-grained fluvial channel sand (core MRM13-CR0101, core depth of 60.64–60.70 m). Potassium feldspar (stained for identification) are partly altered to kaolinite along cleavage (areas noted 1 and 2), some kaolinite alteration of feldspar is more pervasive (e.g. areas 3 and 4). B) Cryogenic preparation of a coarse-grained channel sand for SEM imaging allows the bitumen to remain in contact with the matrix mineralogy. In this image, only a small area of the sample has been abraded by the microtome blade. Inset box shows the location of C and D where the microtome blade has plucked part of the bitumen from the sample surface and has revealed a kaolinite rim around the quartz grain. Kaolinite on the quartz surface is several micrometres thick and subhedral to rounded in places.

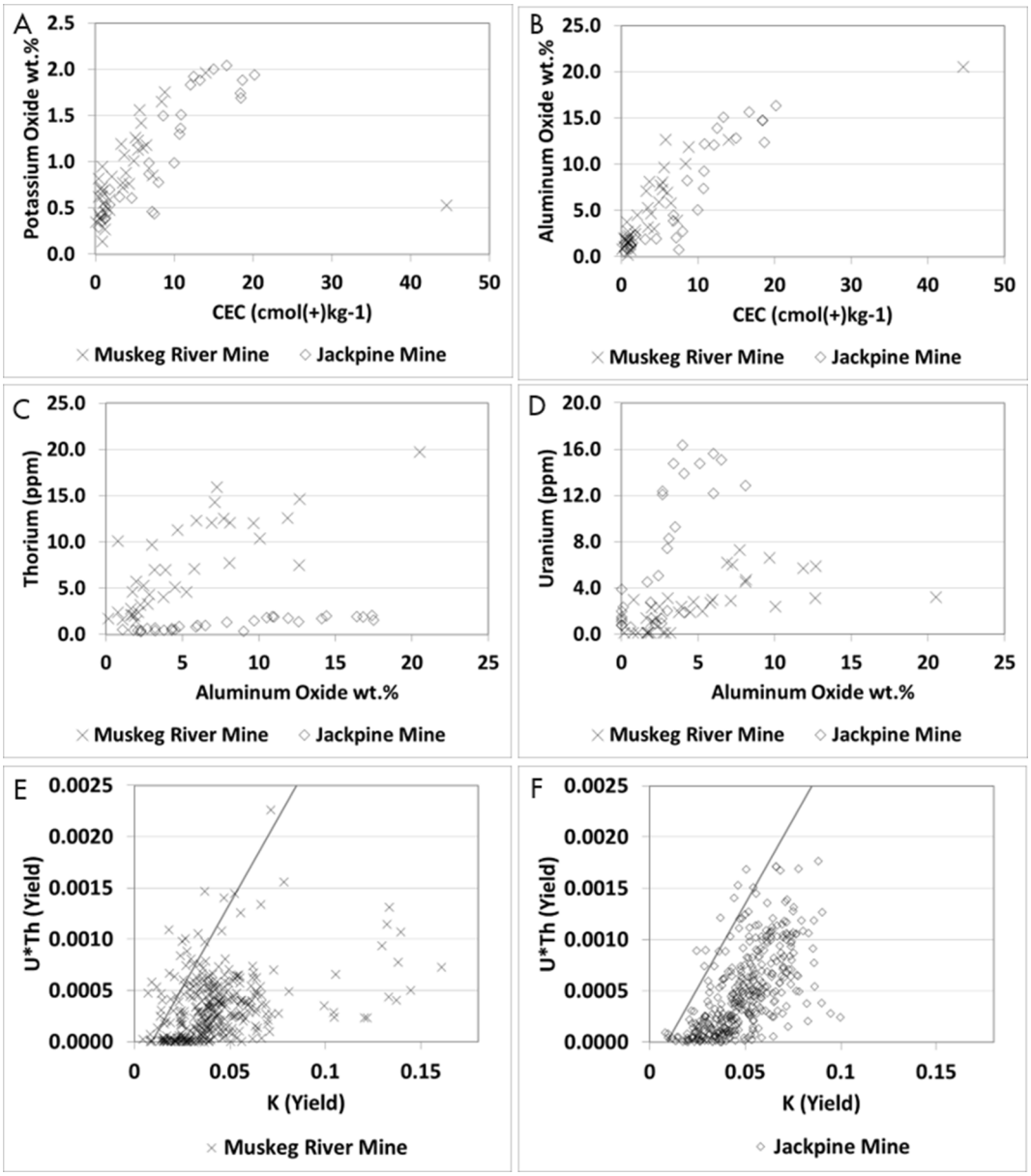

Fig. 7. A-D) Key correlative relationships for significant elements and properties in core data from Muskeg River Mine and Jackpine Mine. E-F) U*Th and K yields from point NGS measurements. Gradient lines (0.035) are defined according to sample stratigraphic position and based on crossing the X-axis > 0.015 potassium yield and placing marsh facies in the Muskeg River Mine core to the left of the line.

McMurray formation (LM1). In LM2, a cycle of low bitumen content is juxtaposed with high bitumen content, that based on core descriptions indicate channel sands filled with bitumen and fine-grained facies with low bitumen charge. The coarse-grained estuarine channel of MM1 is again charged with high bitumen contents, whereas the generally finer-grained inclined heterolithic strata also of MM1 do not contain processable amounts of bitumen. The facies indicator developed above generally shows that when the U*Th and K profiles are aligned with the bitumen indicator the zones of low bitumen contents align with the greatest separation between U*Th and K (Fig. 10).

5. Discussion

In attempting to model the clay size fraction XRD patterns the true complexity of parts of the mineral suite within the McMurray Formation becomes clear (Table 3, Figs. 3 and 5). Complexity aside, reactive mixed-layer clays, manifesting with elevated CEC, in the McMurray Formation are variable and are probably related to different clay formation processes. The lower McMurray Formation has kaolinite-expandable mixed-layer minerals juxtaposed with low expandable (≈20%) illite-smectite. Presumably the low expandability illite-smectite is a detrital component inherited from the source terrain because no high-temperature diagenetic events (typically the route to the formation of illite/smectite of this type) are recorded, e.g., quartz cementation, whereas the kaolinite-expandable mixed-layer mineral is most likely the result of clay mineral transformation or neoformation processes acting at, or soon after, deposition. Indeed, in this context it is notable that almost all occurrences of kaolinite-expandable mixed-layer minerals in both modern and ancient environments are associated with soils or paleosols [33]. As such it seems reasonable to speculate that post depositional soil forming processes probably played a major role in the formation of the kaolinite-expandable mixed-layer mineral in the fluviatile/marsh environments that prevailed during deposition of the Lower McMurray Formation.

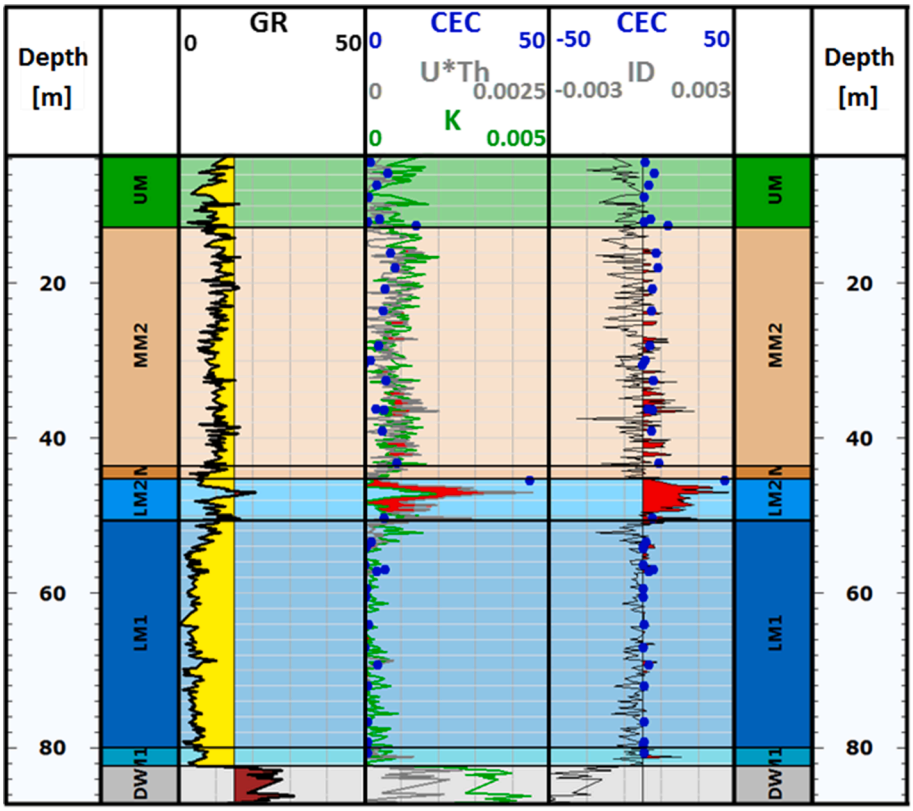

Fig. 8. K, U, Th indicator points to LM2 (marsh facies) as a zone containing problematic minerals independently confirmed by mineralogy and CEC for the Muskeg River Mine core. Blue dots are measured CEC or K, U, Th from XRF data. Continuous lines are interpolated NGS point measurements for the MRM13 Cr0101 core and the red fill highlights zones of maximum separation between K and U*Th yield.

The middle McMurray Formation with low CEC and low expandable illite-smectite appears to represent the inherited mineralogy from the source terrain. By contrast, the upper McMurray Formation appears to have a marine input and this may explain the presence of illite-smectite of relatively high expandability. These factors combine to yield a charged clay profile that manifests as low CEC at the base of the McMurray Formation, transitioning into a zone at the base of the middle McMurray Formation where CECs may be very high. The expandable component of clay minerals in this zone is of more vermiculitic than smectitic character, i.e. higher layer charge which is consistent with the high CEC. Furthermore, it is still not entirely clear if the 14.2 Å reflection which occurs in common association with the kaolinite-expandable mixed-layer mineral (Figs. 4 and 5), is due simply to an associated discrete vermiculitic phase, or is more intimately linked to the kaolinite-expandable mixed-layer mineral (for example by some degree of segregation in the mixed-layering sequences). Probably it is some combination of both options. Thus, despite the expandable clays distinct characteristics to some extent the exact phases are still rather enigmatic, however, high charge characteristics (elevated CEC) and mixed-layering are apparent both of which indicate that these are potentially very reactive clays and their affinity for charged polar molecules. Further, the clay minerals in LM2 and parts of MM1 are characterized by a mineral suite that favors U and Th over K, pointing to the more general kaolinitic signature. Overall, K_2O is not completely diagnostic of the clay mineralogy within the McMurray Formation, as potassium feldspar contributes to its total and a significant portion of clay minerals are non-potassium bearing. In practical terms this suggests that processes to extract bitumen from this material may liberate less bitumen for extraction as, presumably, there is an affinity for the polar molecules in bitumen for these charged sites in clay minerals. As a result, it is also likely that clays will either stay adhered to bitumen and pass to the refinery or pass via a tailings stream to tailings ponds. Both outcomes are not desirable.

The facies indicator developed using K, U, and Th yields from NGS measurements (Fig. 10) has highlighted a separation between the potassium profile with that of U*Th for marsh (broadly LM2) subfacies. It is presumed that potassium yield tracks with total clay content (but also including K-feldspar content) and that U*Th tracks with increasing CEC. Given the mineralogy, where there are few potassium bearing minerals in the LM2 zone, the separation between the K and U*Th profile is dictated by uranium and thorium contents. Specifically, Th resides in kaolinite and U is associated with any organics [50,15]. In the Muskeg River Mine (Fig. 7c), Th content correlates with aluminum and is dictated by kaolinite content. Using the Schlumberger [50] methodology the Muskeg River Mine core data sits on a Th/K line between kaolinite and smectite, whereas the Jackpine Mine core data is more dominated by illite. These observations are consistent with the broad mineralogy of the McMurray Formation. Conversely, the Jackpine Mine core indicated that Th is much lower. When U is compared in the same way the Muskeg River Mine core data has lower U than the Jackpine Mine. It is presumed that uranium is not associated with uranium salts but was adsorbed in the original source rock kerogen material and then remained associated with organics during migration and subsequent biodegradation. Alternatively, at deposition a small kerogen component formed and sequestered U. Regardless of origin, Uranium is now adsorbed onto clay surfaces and contributes to the total gamma-ray count of the formation. By combining the U and Th response both the kaolinite content and clay charge associations are captured.

Where the clay content is highest (Fig. 10) the bitumen contents are lowest, presumably related to lower permeability in the clay rich zones limiting initial hydrocarbon charge prior to biodegradation. At around 65 m in the MRM14 Cr0008 core there is a large separation between the K and U*Th profiles suggesting that this zone has a high clay content, analogous to the marsh facies of LM2. The core descriptions did not

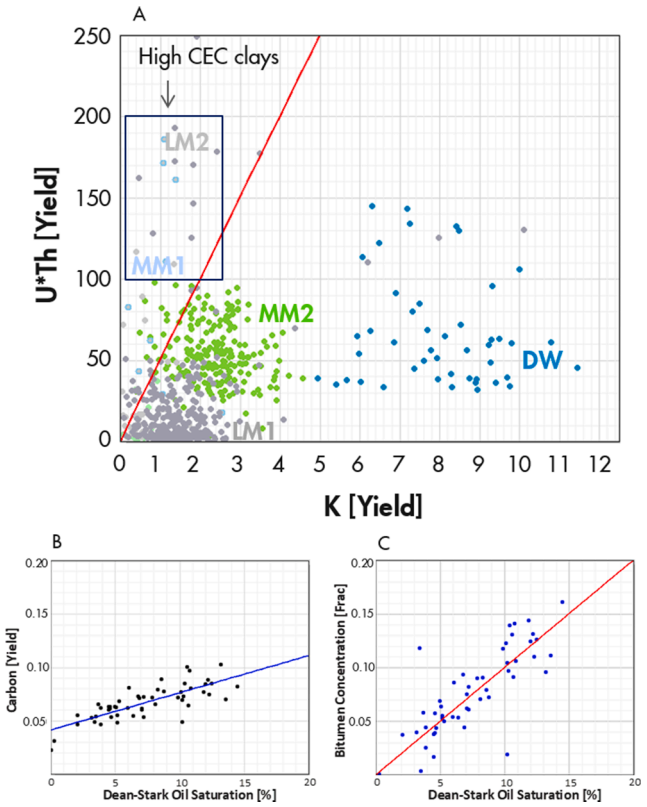

Fig. 9. A) Cross-correlation analysis of U*Th and K field for MRM14 Cr0008 drill hole and core. Gradient of the red line is arbitrarily set to y = 50x. Lower McMurray (LM1 and LM2) and Middle McMurray (MM1 and MM2). Devonian (DW) carbonates. B) Correlation between carbon yield as measured by PNG and C) bitumen concentration in the ore versus Dean-Stark oil saturation for MRM14 Cr0008 core.

identify this zone as potentially a different subfacies, presumably because it was a grain size difference within a mass of bitumen. In other parts of the section covering LM2, the marsh facies stand out clearly where there is low bitumen content and a large separation between U*Th and K from NGS data.

6. Conclusion

Throughout the McMurray Formation quartz is the dominant mineral, however discrete clay minerals (chlorite, muscovite, and kaolinite) were quantified in both bulk and clay size XRD analysis, along with mixed-layered illite-smectite (I-S). Lower and middle McMurray Formation sediments were dominated by I-S with a low expandability, estimated to be 20–30%. Upper McMurray Formation sediments had I-S of higher expandability (60–70%). In floodplain sediments of the lower McMurray Formation an additional mixed-layer mineral has been identified and quantified as a kaolinite-expandable mixed-layer mineral with some vermiculite-like characteristics. The associated CEC values of this kaolinite-expandable mixed-layer mineral are higher than the baseline for the McMurray Formation. More detailed clay mineralogy suggests this kaolinite-expandable mixed-layer is in some cases kaolinite-vermiculite (K-V), with its response to heating and to cation exchange tests pointing to its vermiculitic character. These complex phases with elevated surface charge characteristics probably record a Cretaceous soil forming processes confined to the Lower McMurray Formation resulting in a paleosol.

By combining mineralogy and elemental measurements with laboratory acquired natural gamma-ray spectroscopy (NGS) point measurements, a custom interpretation scheme was transferred to the NGS

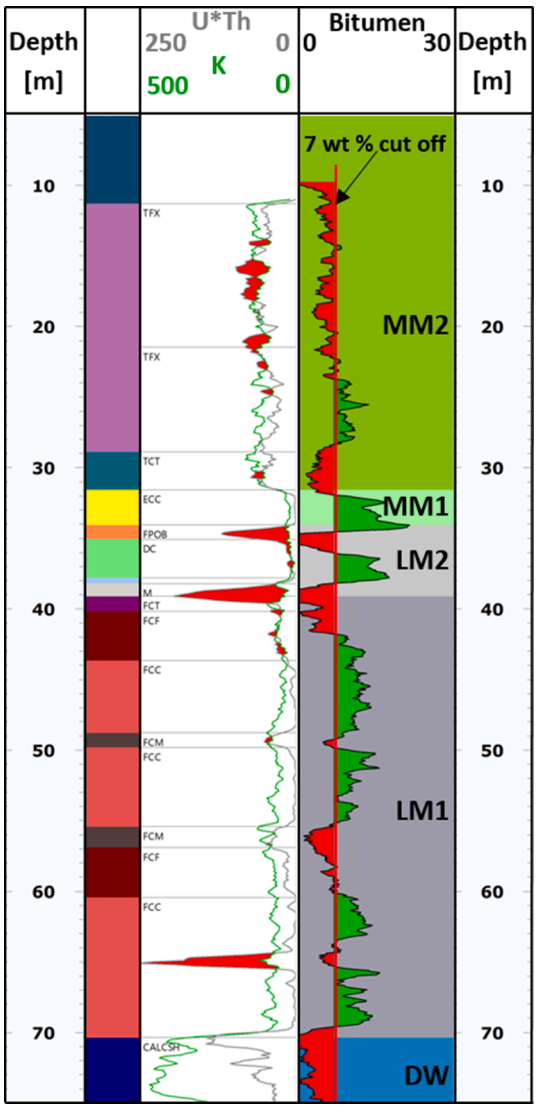

Fig. 10. Carbon indicator combined with U*Th and K indicator to give an ore and mineral breakdown. Maximum separation between K and U*Th (red) are zones with elevated clay mineral surface charge characteristics, threezones are readily resolved by this method to have high clay contents in MRM14 Cr0008. Lower McMurray (LM1 and LM2) and the Middle (MM1 and MM2) and Upper McMurray (UM). Devonian (DW) carbonates sit below the McMurray Formation. The upper McMurray Formation (UM) was not present in this core. Subfacies nomenclature is as follows: Tidal flat mixed (TFX), Tidal channel top (TCT), estuarine channel coarse (ECC), flood plain/overbank (FPOB), Distributary channel (DC), Marsh (M), Fluvial channel top (FCT), Fluvial channel fine (FCF), Fluvial channel coarse (FCC), Fluvial channel margin (FCM), calcareous shale (CALCSH).

logging tool and further developed. The NGS spectra from cores showed that yields of potassium (K), uranium (U), and thorium (Th) had a distinct facies association, that may be explained in terms of clay mineral signatures. Deposition or *in situ* mineral formation appears to dictate elemental partitioning, and thus an indicator was developed that can highlight zones within the ore body that are empirically known to process poorly through the extraction plant. The NGS laboratory learning was extended to a borehole study using a pulsed neutron generator tool (PNG). With the inelastic capture of carbon yield, a bitumen indicator was developed that when combined with NGS spectra allowed a continuous clay and bitumen profile. The developed clay and bitumen indicators were compared to geologic descriptions of core material and were found to highlight zones of low bitumen and high clay

content from the separation between K and U*Th. K_2O or K yield does not adequately quantify the clay content in the orebody, but rather clay content can be assessed by combining U and Th yields. Therefore, spectral gamma-ray is required rather than just total gamma-ray alone to delineate clay contents. Furthermore, the use of K40 analyzers to continuously monitor clay contents through tailings slurry lines may not capture the full clay content being sent to tailings ponds as the kaolinite content is not approximated by this method. However, this study suggests that spectral gamma-ray devices, optimized for use in a mine setting could have utility at any position that requires clay mineral (fines) monitoring, although local calibration with mine specific mineralogy (elements) is critical and this paper provides a framework to achieve this. Based on this study, more rigorous mineralogy acquisition at all stages of mine and plant operation could yield significant value along with the use of NGS and PNG well-logging tools as part of the coring and analysis strategy. Appropriately locally calibrated against mineralogy and elemental data NGS and PNG techniques could be used for in-line, near real-time, instrumentation, at a range of locations around an active mine to monitor ore and tailings streams.

CRediT authorship contribution statement

Ruarri J. Day-Stirrat: Conceptualization, Methodology, Investigation, Visualization, Writing - original draft. **Stephen Hillier:** Formal analysis, Visualization. **Anton Nikitin:** Software, Formal analysis, Investigation, Visualization. **Ronny Hofmann:** Software, Formal analysis, Investigation, Visualization. **Robert Mahood:** Investigation, Data curation. **Gilles Mertens:** Formal analysis, Investigation.

Declaration of Competing Interest

The authors declare that they have no known competing financial interests or personal relationships that could have appeared to influence the work reported in this paper.

Acknowledgments

The authors sincerely thank Shell International Exploration and Production Inc. for permission to publish.

Appendix A. Supplementary data

Supplementary data to this article can be found online at https://doi.org/10.1016/j.fuel.2020.119513.

References

[1] Adams, J., Larter, S., Bennett, B., Huang, H., Westrich, J. & van Kruisdijk, C. (2013) The Dynamic Interplay of Oil Mixing, Charge Timing, and Biodegradation in Forming the Alberta Oil Sands: Insights from Geologic Modeling and Biogeochemistry. Pp. 23-102. In F.J. Hein, D. Leckie, S. Larter, and J.R. Suter, Eds. Heavy-oil and oil-sand petroleum systems in Alberta and beyond,AAPG Studies in Geology 64.
[2] Adriaens R, Vandenberghe N, Elsen J. Natural clay-sized glauconite in the neogene deposits of the campine basin (Belgium). Clays Clay Miner 2014;62:35–52.
[3] Barton MD. The Architecture and variability of valley-fill deposits within the Cretaceous McMurray Formation, Shell Albian Sands Lease, northeast Alberta. Bull Can Pet Geol 2016;64:166–98.
[4] Barton MD, Porter I, O'Byrne C, Mahood R. Impact of the Prairie Evaporite dissolution collapse on McMurray stratigraphy and depositional patterns, Shell Albian Sands Lease 13, northeast Alberta. Bull Can Pet Geol 2016;64:175–99.
[5] Benyon C, Leier AL, Leckie DA, Hubbard SM, Gehrels GE. Sandstone provenance and insights into the paleogeography of the McMurray Formation from detrital zircon geochronology, Athabasca Oil Sands, Canada. AAPG Bull 2016;100:269–87.
[6] Broughton, P.L. (2013a) Depositional Setting and Oil Sands Reservoir Characterization of Giant Longitudinal Sandbars at Ells River: Marginal Marine Facies of theMcMurray Formation,Northern Alberta Basin, Canada. Pp. 313-357. In F.J. Hein, D. Leckie, S. Larter, and J.R. Suter, Eds. Heavy-oil and oil-sand petroleum systems in Alberta and beyond, AAPG Studies in Geology 64.
[7] Broughton PL. Devonian salt dissolution-collapse breccias flooring the Cretaceous Athabasca oil sands deposit and development of lower McMurray Formation sinkholes, northern Alberta Basin, Western Canada. Sed Geol 2013;283:57–82.
[8] Carrigy MA. Geology of the mcmurray formation, part iii: general geology of the mcmurray area. Res Council Alberta Memoir 1959;1:130.
[9] Ciesielski H, Sterckeman T. Determination of cation exchange capacity and exchangeable cations in soils by means of cobalt hexamine trichloride. Agronomie 1997;17:1–7.
[10] Conner A, Chace D, Abou-Saleh J, Kim Y, McNeil C, Gerst J, et al. Developing best practices for evaluating fluid saturations with pulsed neutron capture logging across multiple active CO2-EOR fields. Energy Procedia 2017;114:3636–48.
[11] Cuddy RG, Muwais WK. Channel-fills in the McMurray formation: their recognition, delineation, and impact at the Syncrude mine. Int J Rock Mech Min Sci Geomech Abstracts 1990;27:A106.
[12] Czarnecki J, Radoev B, Schramm LL, Slavchev R. On the nature of Athabasca Oil Sands. Adv Colloid Interface Sci 2005;114–115:53–60.
[13] Dohrmann R, Kaufhold S. Three new, quick CEC methods for determining the amounts of exchangeable calcium cations in calcareous clays. Clays Clay Minerals 2009;57:338–52.
[14] Doveton JH, Merriam DF. Borehole petrophysical chemostratigraphy of Pennsylvanian black shales in the Kansas subsurface. Chem Geol 2004;206:249–58.
[15] Ellis DV, Singer JM. Well logging for earth scientists. Netherlands: Springer; 2007.
[16] Entezari I, Rivard B, Lipsett G. Estimation of methylene blue index in oil sands tailings using hyperspectral data. Can J Chem Eng 2017;95:92–9.
[17] Fustic M, Bennett B, Huang H, Larter S. Differential entrapment of charged oil – New insights on McMurray Formation oil trapping mechanisms. Mar Pet Geol 2012;36:50–69.
[18] Fustic, M., Bennett, B., Hubbard, S.M., Huang, H., Oldenburg, T. & Larter, S. (2013) Impact of Reservoir Heterogeneity and Geohistory on the Variability of Bitumen Properties and on the Distribution of Gas- and Water-saturated Zones in the Athabasca Oil Sands, Canada. Pp. 163-205. In F.J. Hein, D. Leckie, S. Larter, and J.R. Suter, Eds. Heavy-oil and oil-sand petroleum systems in Alberta and beyond,AAPG Studies in Geology 64.
[19] Fustic M, Hubbard SM, Spencer R, Smith DG, Leckie D, Bennett B, et al. Recognition of down-valley translation in tidally influenced meander fluvial deposits, Athabasca Oil Sands (Cretaceous), Alberta, Canada. Mar Pet Geol 2012;29:219–32.
[20] Geramian M, Osacky M, Ivey DG, Lui Q, Etsell TH. Effect of swelling clay minerals (montorillonite and illite-smectite) on nonaqueous bitumen extraction from Alberta Oil Sands. Energy Fuels 2016;30:8083–90.
[21] Gould KM, Piper DJW, Pe-Piper G, MacRae RA. Facies, provenance and paleoclimate interpretation using spectral gamma logs: Application to the Lower Cretaceous of the Scotian Basin. Mar Pet Geol 2014;57:445–54.
[22] Gray N, Lumsdon DG, Hillier S. Effect of pH on the cation exchange capacity of halloysite nanotubes. Clay Miner 2016;51:373–83.
[23] Hein FJ. The cretaceous mcmurray oil sands, Alberta, Canada. Dev Sedimentol 2015;68:561–621.
[24] Hein, F.J., Fairgrieve, B. & Dolby, G. (2012) A Regional Geologic Framework for the Athabasca Oil Sands, Northeastern Alberta, Canada. Pp. 207-250. In F.J. Hein, D. Leckie, S. Larter, and J.R. Suter, Eds. Heavy-oil and oil-sand petroleum systems in Alberta and beyond,AAPG Studies in Geology 64.
[25] Hein, F.J., Leckie, D., Larter, S. & Suter, J.R. (2013) Heavy Oil and Bitumen Petroleum Systems in Alberta and Beyond: The Future Is Nonconventional and the Future Is Now. Pp. 1-21. In F.J. Hein, D. Leckie, S. Larter, and J.R. Suter, Eds. Heavyoil and oil-sand petroleum systems in Alberta and beyond,AAPG Studies in Geology 64.
[26] Hillier S. Use of an air brush to spray dry samples for X-ray powder diffraction. Clay Miner 1999;34:127–35.
[27] Hillier, S. (2002) Spray drying for X-ray powder diffraction preparation. IUCR Commission on Powder Diffraction Newsletter 27, 7-9.
[28] Hillier S. Quantitative analysis of clay and other minerals in sandstones by X-ray powder diffraction (XRPD). In: Worden RH, Morad S, editors. International Association of Sedimentologists Special Publication 34: Clays and Clay cements in Sandstones. Oxford: Blackwell; 2003. p. 213–51.
[29] Hillier, S., Price, R. & Roe, M. (2002) Mixed-layer kaolinite-smectite from the Jurassic Blisworth Clay, Northamptonshire. 18th General Meeting of the International Mineralogical Association, 1-6 September, Edinburgh, Scotland, , Abstracts and Program, P. 165.
[30] Hooshiar A, Uhlik P, Ivey DG, Liu Q, Etsell TH. Clay minerals in nonaqueous extraction of bitumen from Alberta oil sands: Part 2. Characterization of clay minerals. Fuel Process Technol 2012;96:183–94.
[31] Hubert F, Caner L, Meunier A, Ferrage E. Unraveling complex <2μm clay mineralogy from soils using X-ray diffaction profile modeling on particle-size subfractions: implications for soil pedogenesis and reactivity. Am Mineral 2012;97:384–98.
[32] Hubert F, Caner L, Meunier A, Lanson B. Advances in characterization of soil clay mineralogy using X-ray diffraction: from decomposition to profile fitting. Eur J Soil Sci 2009;60:1093–105.
[33] Hughes, R.E., Moore, D.M. & Reynolds, R.C.J. (1993) The nature, occurrence and origin of kaolinite/smectite. . Pp. 291-323. In H. Murray, W. Bundy, and C. Harvey, Eds. Kaolin genesis and utilisation, Special Publication No. 1. Clay Minerals Society, Boulder Colorado.
[34] Hutcheson AL, Grove JE, Mitchell LJ, Phlips BF, Woolf RS, Wulf EA. Effects of rain and soil moisture on background neutron measurements with the SuperMISTI neutron array. Radiat Meas 2017;99:50–9.
[35] Ignasiak TM, Kotlyar L, Longstaffe FJ, Strausz OP, Montgomery DS. Separation and characterization of clay from Athabasca asphaltene. Fuel 1983;62:353–62.
[36] Jackson ML. Soil chemistry analysis advanced course. 2nd Edition. Edition: Published by the author; 1974.

[37] Martinius AW, Fustic M, Garner DL, Jablonski BVJ, Strobl RS, MacEachern JA, et al. Reservoir characterization and multiscale heterogeneity modeling of inclined heterolithic strata for bitumen-production forecasting, McMurray Formation, Corner, Alberta, Canada. Mar Pet Geol 2017;82:336–61.
[38] Mertens, G., Reynolds III, R.C.R. & Adriaens, R. (2016) NEWMOD-2 - A Computer Program for Qualitative and Quantitative 1-D X-ray Diffraction Pattern Modeling. Pp. Fifth EAGE Shale Workshop, 2-4 May 2016, Catania, Italy.
[39] Moore DM, Reynolds RCJ. X-ray diffraction and the identification and analysis of clay minerals. 2 Edition. Oxford, New York: Oxford University Press; 1997.
[40] Musial G, Reynaud J-Y, Gingras MK, Féniès H, Labourdette R, Parize O. Subsurface and outcrop characterization of large tidally influenced point bars of the cretaceous mcmurray formation (Alberta, Canada). Sed Geol 2012;279:156–72.
[41] Nagy B, Gagnon GC. The geochemistry of the Athabasca petroleum deposit. I. Elution and spectroscopic analysis of the petroleum from the vicinity of McMurray, Alberta. Geochim Cosmochim Acta 1961;23:155–85.
[42] Nardin, T.R., Feldman, H.R. & Carter, B.J. (2012) Stratigraphic Architecture of a Large-scale Point-bar Complex in the McMurray Formation: Syncrude's Mildred Lake Mine, Alberta, Canada. Pp. 273-311. In F.J. Hein, D. Leckie, S. Larter, and J.R. Suter, Eds. Heavy-oil and oil-sand petroleum systems in Alberta and beyond, AAPG Studies in Geology 64.
[43] North CP, Boering M. Spectral Gamma-ray logging for facies discrimination in mixed fluvial-eolian successions: a cautionary tale. AAPG Bull 1999;83:155–69.
[44] Omotoso O, McCarty DK, Hillier S, Kleeberg R. Some successful approaches to quantitative mineral analysis as revealed by the 3rd Reynolds Cup contest. Clays Clay Miner 2006;54:748–60.
[45] Omotoso OE, Mikula RJ. High surface areas caused by smectitic interstratification of kaolinite and illite in Athabasca oil sands. Appl Clay Sci 2004;25:37–47.
[46] Omotoso OE, Mikula RJ, Stephens PW. Surface area of interstratified phyllosilicates in Athabasca oil sands from synchrotron XRD. JCPDS-Int Centre Diff Data Adv X-ray Anal 2002;45:391–6.
[47] Osacky M, Geramian M, Ivey DG, Lui Q, Etsell TH. Mineralogical and chemical composition of petrologic end members of Alberta oil sands. Fuel 2013;113:148–57.
[48] Osacky M, Geramian M, Ivey DG, Lui Q, Etsell TH. Influence of nonswelling clay minerals (illite, kaolinite, and chlorite) on noncqueous solvent extraction of bitumen. Energy Fuels 2015;29:4150–9.
[49] Sakharov BA, Lindgreen H, Salyn H, Drits VA. Determination of illite-smectite structures using multispecimen X-ray profile fitting. Clays Clay Miner 1999;47:555–66.
[50] Schlumberger. (1985) Interpretation charts. Schlumberger, New York.
[51] Wang S, Xiao L, Yue A, Wang H, Liu W, Fan Y. Accurate inversion of elemental concentrations from the pulsed neutron geochemical logging based on an active-set method. J Petrol Sci Eng 2017;157:833–41.
[52] Yu H, Sun J, Wang J, Gardner RP. Accuracy and borehole influences in pulsed neutron gamma density logging while drilling. Appl Radiat Isot 2011;69:1313–7.
[53] Zhang F, Zhang Q, Liu J, Wang X, Wu H, Jia W, et al. A method to describe inelastic gamma field distribution in neutron gamma density logging. Appl Radiat Isot 2017;129:189–95.